Paleoceanography and Paleoclimatology

RESEARCH ARTICLE
10.1029/2017PA003304

Twentieth Century Seawater $\delta^{18}O$ Dynamics and Implications for Coral-Based Climate Reconstruction

S. Stevenson[1], B. Powell[2], K. M. Cobb[3], J. Nusbaumer[4], M. Merrifield[5], and D. Noone[6]

[1]Bren School of Environmental Science and Management, University of California, Santa Barbara, CA, USA, [2]Department of Oceanography, University of Hawai'i, Honolulu, HI, USA, [3]Department of Earth and Atmospheric Sciences, Georgia Institute of Technology, Atlanta, GA, USA, [4]NASA Goddard Institute for Space Studies, NY, USA, [5]Integrative Oceanography Division, Scripps Institution of Oceanography, University of California, San Diego, La Jolla, CA, USA, [6]College of Earth, Ocean, and Atmospheric Sciences, Oregon State University, Corvallis, OR, USA

Key Points:
- Salinity and seawater $\delta^{18}O$ variations are not always well correlated, and their relationship is affected by ENSO dynamics
- The salinity:seawater $\delta^{18}O$ relationship varies strongly on interannual time scales
- Reconstructing salinity based on seawater $\delta^{18}O$ may have large uncertainties

Correspondence to:
S. Stevenson,
sstevenson@ucsb.edu

Citation:
Stevenson, S., Powell, B., Cobb, K. M., Nusbaumer, J., Merrifield, M., & Noone, D. (2018). Twentieth century seawater $\delta^{18}O$ dynamics and implications for coral-based climate reconstruction. *Paleoceanography and Paleoclimatology*, *33*, 606–625. https://doi.org/10.1029/2017PA003304

Received 11 DEC 2017
Accepted 4 APR 2018
Accepted article online 20 APR 2018
Published online 20 JUN 2018
Corrected 23 MAY 2019

This article was corrected on 23 MAY 2019. See the end of the full text for details.

Abstract The oxygen isotopic composition of tropical coral skeletons ($\delta^{18}O$) is a crucial source of information on past El Niño/Southern Oscillation behavior. Both temperature and the $\delta^{18}O$ of the surrounding seawater ($\delta^{18}O_{sw}$) affect coral $\delta^{18}O$; a linear proportionality with $\delta^{18}O_{sw}$ is often used to infer past salinity variations, but the degree to which dynamical influences on $\delta^{18}O_{sw}$ may affect that relationship is still unclear. Here we use the isotope-enabled Regional Ocean Modeling System to investigate the dynamics of $\delta^{18}O_{sw}$ and salinity variations in different twentieth century climate regimes. The dominant modes of $\delta^{18}O_{sw}$ variability are the background trend and eastern/central Pacific El Niño, similar to salinity; likewise, budget analysis reveals a strong impact of ocean dynamics (both advection and vertical mixing/diffusion) on $\delta^{18}O_{sw}$ variations during El Niño and La Niña events. These dynamics lead to alterations in the $\delta^{18}O_{sw}$:salinity relationship across the Pacific: the linear approximation is most accurate near the eastern edge of the western Pacific warm pool but with nonlinearities due to large $\delta^{18}O_{sw}$ excursions during El Niño. At other sites, the $\delta^{18}O_{sw}$:salinity relationship has substantial scatter and explains relatively little $\delta^{18}O_{sw}$ variance. Strikingly, interannual variability can lead to site-specific $\delta^{18}O_{sw}$:salinity regression coefficient changes of up to 0.4‰/psu on multiyear time scales. This calls the reliability of coral-based estimates of El Niño/Southern Oscillation extremes into question and highlights the need for increased dynamical understanding as well as sustained in situ observations of $\delta^{18}O_{sw}$ and salinity variability.

Plain Language Summary Tropical corals record past El Niño and La Niña events through changes in the isotopic ratios of oxygen in their skeletons, which is affected by the isotopic composition of seawater local to the reef. This seawater $\delta^{18}O$ is thought to be closely related to salinity and is used to reconstruct past salinity variations associated with El Niño. However, this paper uses an isotope-enabled ocean model to show that salinity and seawater $\delta^{18}O$ have a complicated relationship. The processes affecting the two variables can be quite different in places, and their relationship varies significantly with time; therefore, it may be much more difficult to use coral records to reconstruct past salinity changes (and thus, El Niño impacts) than was previously thought.

1. Introduction

The El Niño/Southern Oscillation (ENSO) dominates interannual climate variability and impacts human and natural systems around the world (Di Lorenzo & Mantua, 2016; Ropelewski & Halpert, 1987). Its response to anthropogenic climate change is thus a critical question, but as of yet climate model projections of 21st century ENSO behavior vary widely (Bellenger et al., 2014; Collins et al., 2010; Guilyardi et al., 2009; Stevenson, 2012). In order to understand the physical drivers of climate change impacts on ENSO dynamics, a multicentennial observational ENSO baseline is needed to mitigate the influence of internal variability and forcing uncertainties (Stevenson et al., 2010, 2012; Wittenberg, 2009). This necessitates the use of paleoclimate information to extend the instrumental record.

The isotopic ratio of oxygen in the aragonitic skeletons of tropical coral reefs ($\delta^{18}O$) is a sensitive recorder of past ENSO variability; coral reefs are often located near the peak of ENSO-related sea surface temperature (SST) anomalies, and their high growth rates enable individual El Niño and La Niña events to be reconstructed.

As such, coral $\delta^{18}O$ has been used extensively to infer past ENSO characteristics (e.g., Cobb et al., 2003; Cole et al., 1993; Linsley et al., 1994; McGregor et al., 2011; Quinn et al., 2006). However, a detailed mechanistic interpretation of coral $\delta^{18}O$ can be difficult, as coral $\delta^{18}O$ is governed by both changes in temperature, which alters $\delta^{18}O$ through inorganic aragonite precipitation (Epstein et al., 1953; Fairbanks et al., 1997), and changes in the ambient $\delta^{18}O$ of seawater in the coral environment ($\delta^{18}O_{sw}$). This leads to often substantial differences in the balance of processes affecting coral $\delta^{18}O$ at different locations as a function of ENSO phase (Stevenson et al., 2015), even when biologically driven uncertainties are neglected (e.g., Carilli et al., 2013).

In order to enable the quantitative use of $\delta^{18}O$-based ENSO diagnostics, accurate estimates of ENSO characteristics based on their $\delta^{18}O$ signatures are required. This requires some form of conversion between a relevant metric of ENSO and local temperature/$\delta^{18}O_{sw}$ parameter space, which may be performed "online" within a climate model framework, by directly incorporating oxygen isotopes into general circulation models (Russon et al., 2013; Schmidt et al., 2007; Werner et al., 2016; Zhu et al., 2017). However, the majority of general circulation model simulations do not include this capacity, and it is often desirable to perform evaluations using observational data as well. To enable comparison against coral data in such cases, "forward model" conversions between local physical conditions and coral $\delta^{18}O$ have been employed in previous studies (Dee et al., 2016; Thompson et al., 2011). The temperature component of the model is relatively straightforward, relying on the temperature dependence of inorganic aragonite deposition (Epstein et al., 1953; Fairbanks et al., 1997). However, forward modeling $\delta^{18}O_{sw}$ is quite complex; the approach to date relies on the covariance between salinity and $\delta^{18}O_{sw}$ to predict the $\delta^{18}O_{sw}$ component of coral $\delta^{18}O$ using linear regression against local salinity (Brown et al., 2008; LeGrande & Schmidt, 2006; Thompson et al., 2011). Although this approach works as a first approximation, in reality the processes affecting $\delta^{18}O_{sw}$ may be distinct from those governing salinity variations (Stevenson et al., 2015), and the associated errors can in fact lead to uncertainties of 50% or more on the forward modeled coral $\delta^{18}O$ variance (Stevenson et al., 2013).

Improving forward models of seawater $\delta^{18}O$ is crucial for improving ENSO reconstructions; since such models currently rely to a large extent on the relationship between salinity and seawater $\delta^{18}O$, it is therefore also crucial to understand the controls on these relationships. To date, the extreme sparsity of seawater $\delta^{18}O$ data has prevented the comprehensive analysis of the S:$\delta^{18}O_{sw}$ relations; only a few observations are available at any given location (LeGrande & Schmidt, 2006). Nonetheless, it is well established that substantial regional structure exists in the salinity:seawater $\delta^{18}O$ relation (Conroy et al., 2014, 2017; LeGrande & Schmidt, 2006). The recent construction of the isotope-enabled Regional Ocean Modeling System (isoROMS; Stevenson et al., 2015) is designed to address this knowledge gap, by creating a spatially and temporally complete set of salinity and seawater $\delta^{18}O$ data covering as long a time period as possible. The Regional Ocean Modeling System (ROMS) has the capacity to simulate circulation on arbitrarily fine scales, and the inclusion of oxygen isotope tracers allows isoROMS to serve as an estimate of twentieth century $\delta^{18}O_{sw}$ variations (an approximation of the fields which might result from a reanalysis). A proof of concept study with isoROMS showed the utility of the model over the late twentieth century (Stevenson et al., 2015); here we present results from a new isoROMS simulation with increased temporal extent and spatial resolution.

2. Experimental Setup

2.1. ROMS Configuration

ROMS is a free-surface, terrain-following ocean model that uses a split-explicit time-stepping algorithm (Shchepetkin & McWilliams, 2005) and has been employed to simulate a variety of island environments (Janeković et al., 2013; Souza et al., 2015), including the impact of local circulation on $\delta^{18}O_{sw}$ near the Line Islands (Stevenson et al., 2015). Here we use a slightly updated version of the isoROMS configuration described in Stevenson et al. (2015); the representation of seawater $\delta^{18}O$ takes advantage of ROMS' native passive tracer simulation capacity, with evaporative fractionation computed using the scheme developed by Merlivat and Jouzel (1979). This approach is described for isoROMS in detail by Stevenson et al. (2015) and follows methods commonly used in isotope-enabled general circulation models (Noone & Simmonds, 2002; Nusbaumer et al., 2017; Schmidt et al., 2005).

The present ROMS grid is similar to the Pacific-wide simulation described in Stevenson et al. (2015), covering the entire Pacific basin north of 30°S but with increased resolution near the equator to allow improved simulation of small-scale features. The vertical resolution has also been increased relative to Stevenson et al. (2015), from 15 to 30 levels. This increase is most pronounced in the upper few

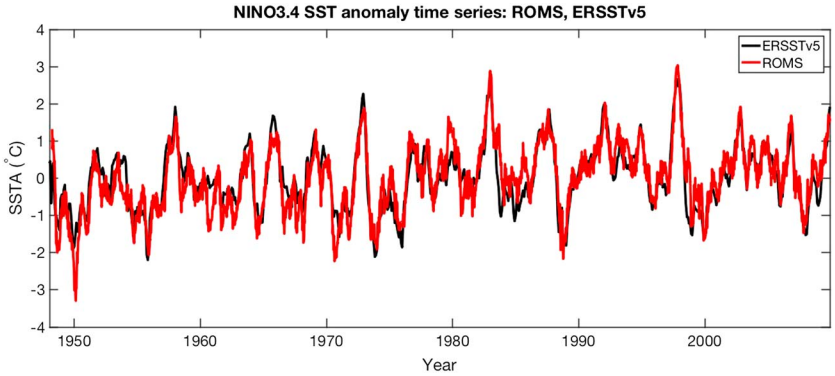

Figure 1. Performance of NINO3.4 sea surface temperature (SST) anomaly in Regional Ocean Modeling System (ROMS) relative to Extended Reconstructed Sea Surface Temperature version 5 (ERSSTv5).

hundred meters of the water column, enabling a more accurate representation of mixing and diffusion of surface-driven precipitative/evaporative fluxes. As in Stevenson et al. (2015), surface boundary conditions for most physical quantities (heat flux, wind stress, sea level pressure, and air temperature/humidity) are derived from the Common Ocean-Ice Reference Experiment, Phase II (CORE2) data set of Large and Yeager (2008), and seawater isotopologue concentrations are initialized from the time-mean product of LeGrande and Schmidt (2006).

The use of the isotope-enabled configuration of ROMS requires the specification of the isotopic composition of precipitation (we note that potential influences from water vapor isotopic exchange are here neglected, as equilibrium between precipitation and the surrounding vapor is assumed; Merlivat & Jouzel, 1979). The isotopic composition of precipitation is generally not well constrained observationally, although a limited amount of data has been collected by the Global Network of Isotopes in Precipitation project (Rozanski et al., 1993) as well as other targeted investigations (Bailey et al., 2013; Conroy et al., 2016; Moerman et al., 2013). To provide the necessary input field for isoROMS, we use precipitation δ^{18}O values taken from a twentieth century simulation using the isotope-enabled version of the Community Atmosphere Model version 5 (iCAM5; Nusbaumer et al., 2017). This allows the inclusion of seasonal and interannual variations in precipitation δ^{18}O; seasonal variations in precipitation δ^{18}O are well represented in iCAM5 (Nusbaumer et al., 2017), while interannual variations are more difficult to validate owing to the lack of continuous observational data.

The treatment of freshwater exchanges between the atmosphere and ocean (e.g., evaporation and precipitation) differs in this study from Stevenson et al. (2015). Rather than simply imposing the *E-P* field from the German contribution to the Estimating the Circulation and Climate of the Ocean project (GECCO2) state estimate, the present simulation employs a two-step process designed to provide optimal representation of salinity while allowing the use of precipitative isotopologue fluxes from iCAM. An initial experiment over the CORE2 period (1948–2009) was performed with *E-P* prescribed from GECCO2 and applying a correction term to the freshwater flux to improve salinity performance (a so-called "salt flux correction"; see also Stevenson et al., 2015). From this simulation, the evaporation field output from ROMS and the iCAM precipitation field were then combined to create a new freshwater flux, and a free-running simulation was performed with this new flux prescribed over the 1948–2009 period. This approach ensures that the net surface freshwater flux and surface isotopic balance are consistent while maintaining the mean and background trends in salinity consistent with GECCO2; as such, this is an improvement over the artificial decoupling introduced by the method of Stevenson et al. (2015).

2.2. Model Validation

The performance of the production run is evaluated relative to both physical and geochemical observations. The NINO3.4 SST anomaly has been computed for the ROMS production run (Figure 1); when anomaly time series are compared between ROMS and Extended Reconstructed Sea Surface Temperature Version 3b (ERSSTv3b), the correlation is 0.86. The absolute temperature time series also correlates extremely well with ERSSTv3b ($R^2 = 0.89$; not pictured), despite slight biases toward cold conditions earlier in the run, likely related to adjustment between the atmospheric forcing and initial ocean state. isoROMS captures the mean structure of $\delta^{18}O_{sw}$ quite well, as evidenced by the similar patterns in climatological-mean $\delta^{18}O_{sw}$ between isoROMS and the LeGrande and Schmidt (2006) product over 1980–2009 (Figure 2).

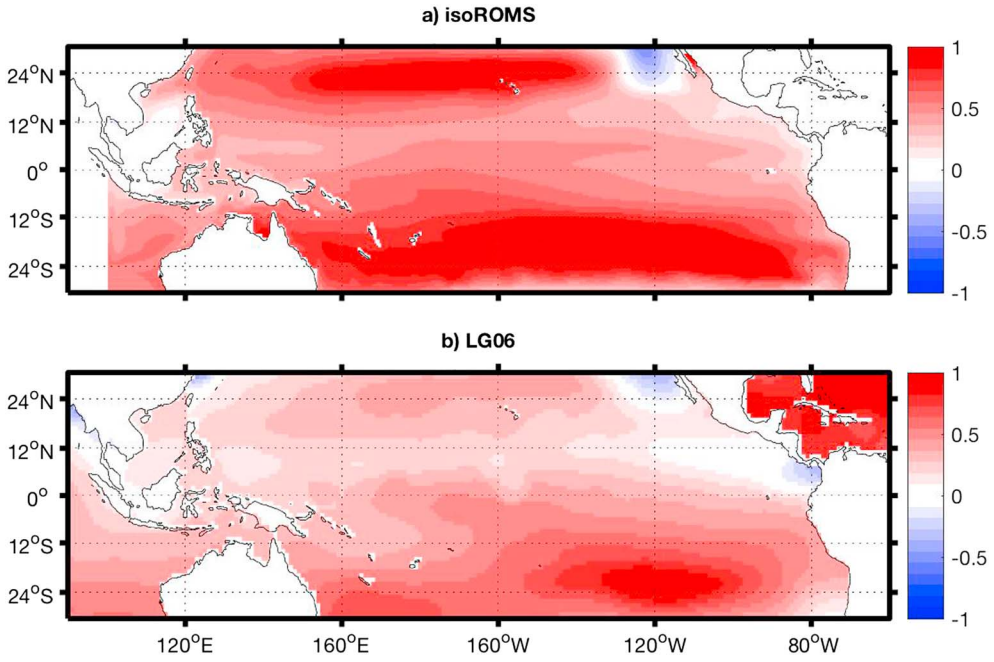

Figure 2. Climatological mean $\delta^{18}O_{sw}$ in (a) isotope-enabled Regional Ocean Modeling System (isoROMS) and (b) the LG06 data set over 1980–2009.

To validate isoROMS performance at proxy sites, we focus on Pacific locations with multidecadal coral $\delta^{18}O$ time series sampled at seasonal or higher temporal resolution; the total list of sites is given in Table 1. Temperature and salinity performance at the study sites is roughly comparable to the isoROMS simulation used in Stevenson et al. (2015). The R^2 values for temperature are on the order of 0.7 for sites in the central equatorial Pacific and 0.8 to 0.9 in locations in the southwest Pacific where the seasonal cycle is the dominant time scale. Performance is less accurate in the western equatorial Pacific, but the R^2 values are still generally above 0.4. As was the case in Stevenson et al. (2015), the representation of salinity is less accurate than temperature, with the maximum R^2 value near 0.7; we anticipate that the correspondence between isoROMS salinity may be higher using satellite-derived estimates, but this was not possible given the end point of 2009 for the current simulations. Salinity is generally best represented in the western/central equatorial and southwestern Pacific, and the mismatches between GECCO2 and isoROMS salinity estimates are of the same magnitude as those between the GECCO2 and Delcroix et al. (2011) salinity products (not pictured). We thus consider the physical climate within isoROMS relatively well represented.

The $\delta^{18}O_{sw}$ time series from isoROMS are compared with coral-derived values for locations at which paired coral $\delta^{18}O$ and Sr/Ca measurements were available, enabling the computation of seawater $\delta^{18}O$ as the residual of the two (e.g., Cahyarini et al., 2008). Where possible, we have used the seawater $\delta^{18}O$ values computed by the original authors: this is the case for Christmas, Palmyra, and Fanning (Nurhati et al., 2009, 2011). In cases where the raw coral $\delta^{18}O$ and Sr/Ca data were available but the resulting seawater $\delta^{18}O$ had not been made public, we have computed seawater $\delta^{18}O$ following the method of Cahyarini et al. (2008) which relates "centered" (mean removed) SST to Sr/Ca, and coral $\delta^{18}O$ to SST, using empirically derived calibration relationships:

$$\Delta\delta^{18}O_{sw} = (\delta^{18}O_{coral} - \overline{\delta^{18}O_{coral}}) - \frac{\gamma_1}{\beta_1}(Sr/Ca - \overline{Sr/Ca}) \quad (1)$$

Here overbars indicate temporal means, γ_1 is the regression of coral $\delta^{18}O$ versus SST (here assumed equal to −0.21‰/°C), and β_1 the regression slope of Sr/Ca versus SST. The Advanced Very High Resolution Radiometer (AVHRR) Optimum Interpolation Sea Surface Temperature version 2 (OISSTv2) product was used for calibration via least squares regression of local SST onto Sr/Ca during the period from 1981 to the end of the record. Tests in cases where published $\delta^{18}O_{sw}$ was available showed that the $\delta^{18}O_{sw}$ time series calculated here are correlated at 0.95 or above with $\delta^{18}O_{sw}$ time series provided by the original authors (not pictured).

Table 1
Performance of isoROMS at Simulating Temperature, Salinity, Coral $\delta^{18}O$, and Seawater $\delta^{18}O$ at Coral Study Sites Over 1965–2009

Site	R_T	R_S	R_{coral}	R_{sw}	Coral period	Coral reference
Timor	0.86	0.09	0.09	0.07	1965–2004	Cahyarini et al. (2014)
Butaritari	0.58	0.54	0.21	0.10	1965–2009	Carilli et al. (2014)
Maiana	0.62	0.45	0.40	–	1965–1994	Urban et al. (2000)
Nauru	0.47	0.43	0.29	–	1965–1995	Guilderson and Schrag (1999)
Tarawa	0.62	0.45	0.24	–	1965–1990	Cole et al. (1993)
Secas	0.57	0.72	0.02	–	1965–1984	Linsley et al. (1994)
Laing	0.43	0.40	0.11	–	1965–1993	Tudhope et al. (2001)
Madang	0.44	0.44	0.11	–	1965–1991	Tudhope et al. (2001)
Palau	0.67	0.32	0.35	–	1965–2008	Osborne et al. (2014)
Rabaul	0.49	0.33	0.14	0.21	1965–1997	Quinn et al. (2006)
Christmas	0.71	0.35	0.33	0.02	1972–1998	Nurhati et al. (2009)
Fanning	0.74	0.27	0.42	0	1972–2005	Nurhati et al. (2009)
Palmyra	0.71	0.45	0.39	0	1972–1998	Nurhati et al. (2009)
Fiji	0.89	0.43	0.30	–	1965–2001	Linsley et al. (2004)
New Caledonia	0.91	0.41	0.57	0.01	1968–1992	Quinn and Sampson (2002)
Rarotonga	0.91	0.42	0.45	–	1965–1996	Linsley et al. (2006)
Vanuatu	0.89	0.56	0.37	0.17	1965–1992	Kilbourne et al. (2004)

Note. Values given are R^2 between observed data and monthly mean isoROMS output averaged over a 2° × 2° box surrounding each proxy site (temperature and salinity) or from the grid point closest to the coral site ($\delta^{18}O$). Data sources are ERSSTv5 for temperature (R_T), GECCO2 for salinity (R_S), and coral data described in the text for coral and seawater $\delta^{18}O$ (R_{coral} and R_{sw}). The period used for computing coral and seawater $\delta^{18}O$ coefficients is listed as "Coral period." The original reference for the coral data is listed in the "Coral reference" column.

Table 1 lists R^2 values for coral and seawater $\delta^{18}O$, as specified above. In most cases, the simulation of coral $\delta^{18}O$ is comparable to or somewhat less accurate than the simulation of salinity and are similar to the performance of the isoROMS configuration presented in Stevenson et al. (2015). However, the model's ability to correctly simulate coral $\delta^{18}O$ appears to result in large part from its accurate temperature representation, and in general the model's ability to reproduce the $\delta^{18}O_{sw}$ time series is lower, with $\delta^{18}O_{sw}$ from ROMS exhibiting lower variance than coral-derived $\delta^{18}O_{sw}$ at most sites. The fact that coral $\delta^{18}O$ variance is fairly well represented by ROMS would then suggest the potential for compensating errors in $\delta^{18}O_{sw}$ and temperature; however, tests using ROMS temperature to estimate $\delta^{18}O_{sw}$ by subtraction from coral $\delta^{18}O$ reveal close agreement with coral-derived $\delta^{18}O_{sw}$ (not pictured), indicating that ROMS-derived temperature is not causing these issues. Without a more detailed observational $\delta^{18}O_{sw}$ data set, it is difficult to attribute model/proxy offsets to either true deficiencies in ROMS (e.g., errors in simulation of hydrological processes, vertical mixing, or others) or the uncertainties associated with the computation of $\delta^{18}O_{sw}$ from coral $\delta^{18}O$ and Sr/Ca (e.g., uncertainties in the Sr/Ca:SST calibration coefficient or noncontemporaneous high-frequency noise in the $\delta^{18}O$ and Sr/Ca data sets). Given all of these caveats, the fact that there is considerable shared variance between isoROMS and coral-derived $\delta^{18}O_{sw}$ (see time series in Figures 3 and 4) is an encouraging sign, and we anticipate that future model improvements and refinements in $\delta^{18}O_{sw}$ geochemical estimation will lead to still more accurate simulation of $\delta^{18}O_{sw}$ variations.

2.3. Site Classification

For ease of discussion in later sections, we have classified the set of study sites into several categories based on the prevailing circulation regimes at their locations:

1. *Central Pacific.* These sites all lie within the Line Islands chain, near the longitude of the ENSO center of action. Most have been shown to be dominated by variations in temperature (Cobb et al., 2003, 2013; Nurhati et al., 2011). Nonetheless, seawater $\delta^{18}O$ variations can be important at these sites, particularly during extreme El Niño events; these influences vary from site to site, due to the changing role of ocean

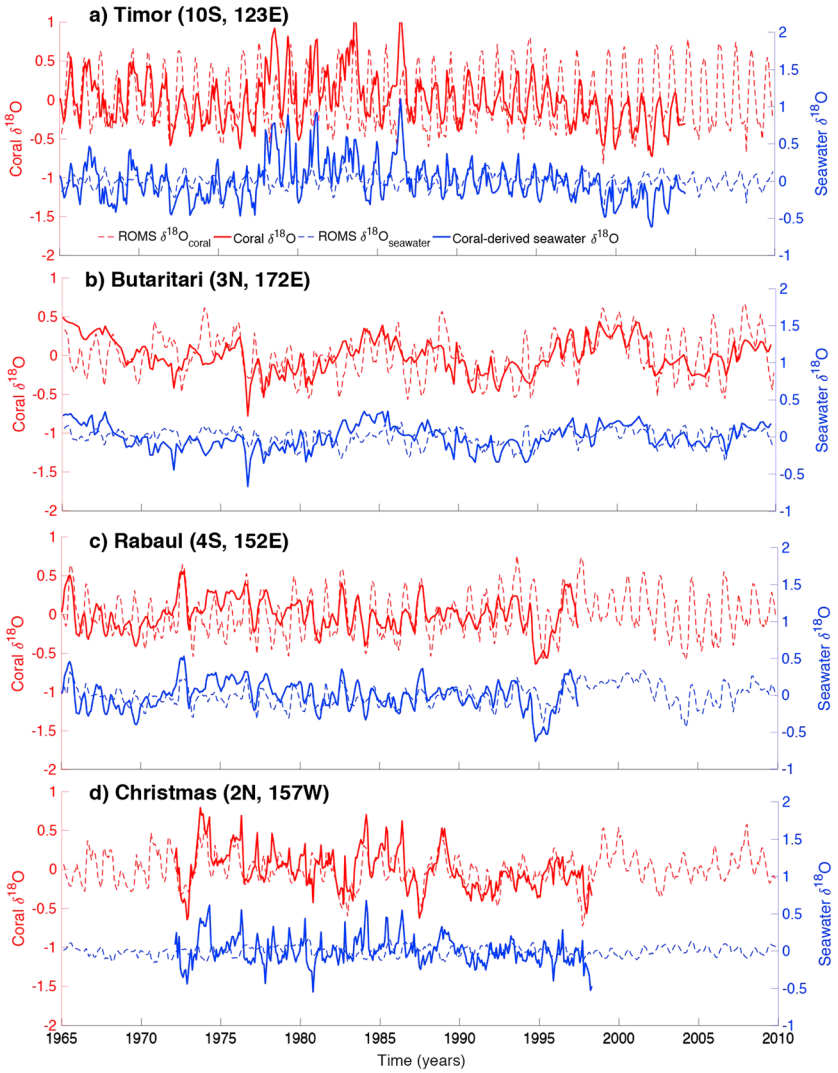

Figure 3. Performance of the Regional Ocean Modeling System (ROMS) at simulating coral $\delta^{18}O$ and coral-derived seawater $\delta^{18}O$ estimates. Solid lines indicate coral-derived observational data, while isotope-enabled ROMS output is shown as dashed lines. (a) Timor; (b) Butaritari; (c) Rabaul; and (d) Christmas.

dynamical processes and impacts from the Intertropical Convergence Zone (ITCZ; McGregor et al., 2011; Nurhati et al., 2009, 2011; Stevenson et al., 2015).

2. *West Central Pacific.* These sites lie near the eastern edge of the warm pool and have been shown to be affected by both temperature and $\delta^{18}O_{sw}$ variations (Carilli et al., 2014; Cole et al., 1993; Urban et al., 2000). Their location west of the ENSO center of action leads to a lag relationship with ENSO phase, and both surface-driven and advective processes have been shown to operate at these sites (Carilli et al., 2014).
3. *East Pacific.* The Galapagos is the only site in this category, lying in the far eastern equatorial Pacific and dominated by temperature variations. We note that this results in possible biases due to site-specific influences but, in the absence of other collocated sites, believe that the uniqueness of the Galapagos warrants its separate classification here. As for the central Pacific sites, precipitative excursions during El Niño can create large $\delta^{18}O_{sw}$ changes; shifts in equatorial upwelling and impacts from the Equatorial Undercurrent are also potentially significant (Karnauskas et al., 2010).
4. *Warm Pool.* These sites lie within the climatological extent of the warm pool, farther west than the west central Pacific sites. They generally experience higher variations in seawater $\delta^{18}O$ relative to temperature (Quinn et al., 2006; Tudhope et al., 2001). The mean precipitation is large at these locations and the thermocline relatively deep. Mean temperature and $\delta^{18}O_{sw}$ gradients are small at these sites, indicating that advective influences should arise primarily from shifts in regional circulation rather than larger-scale patterns.

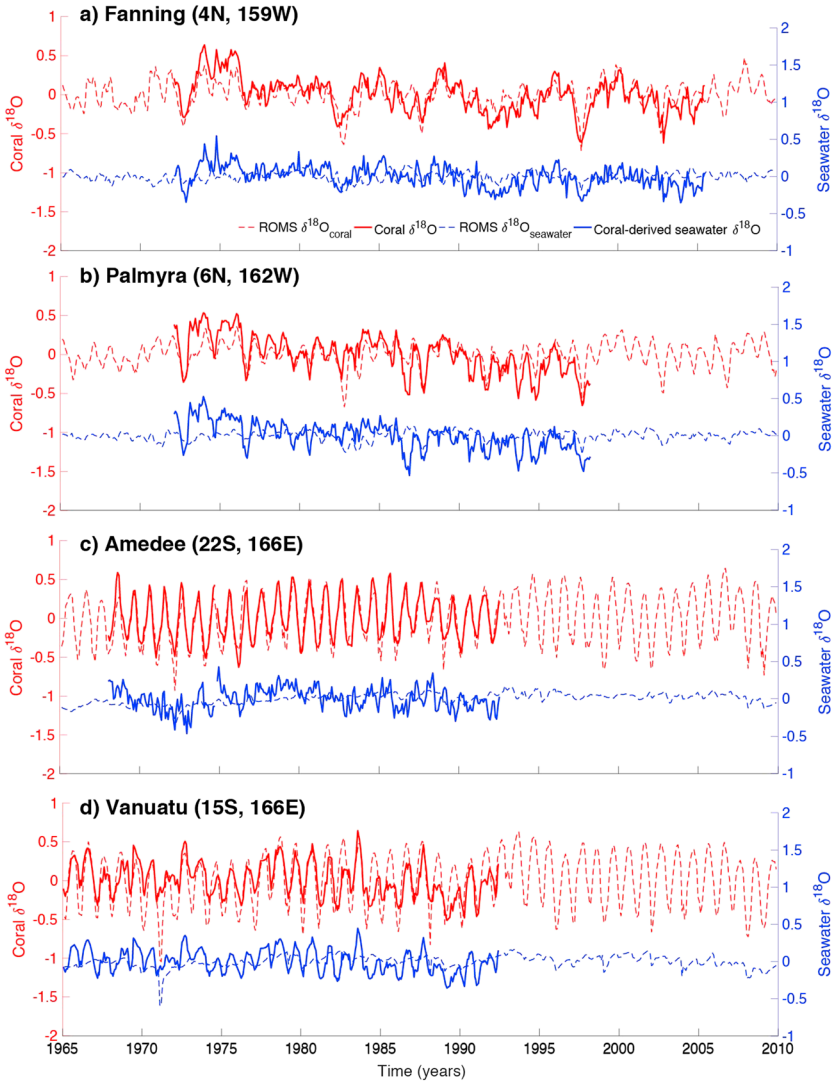

Figure 4. Same as Figure 3, for additional sites. Solid lines indicate coral-derived observational data, while isotope-enabled ROMS output is shown as dashed lines. (a) Fanning; (b) Palmyra; (c) Amedee; and (d) Vanuatu.

5. *Maritime Continent.* These sites are also quite far west but have been separated from the warm pool sites due to their locations in the Indonesian Throughflow (Timor) or proximity to Australia (Flinders and Great Barrier Reef (GBR)). Precipitation is also quite high here, and seawater $\delta^{18}O$ variations are dominant.
6. *Southwest Pacific.* These sites lie in the region of influence of the South Pacific Convergence Zone (SPCZ) and exhibit strong variations in both temperature and seawater $\delta^{18}O$. They span a wide range of longitudes but are not near any major landmasses and have previously been demonstrated to vary coherently both with one another and with salinity fronts associated with the SPCZ (Dassie et al., 2014; Linsley et al., 2006; Wu et al., 2014).
7. *Intertropical Convergence Zone.* These sites lie north of the equator in the central/eastern Pacific and are strongly influenced by seasonal and interannual migrations of the ITCZ. They are dominated by seawater $\delta^{18}O$ to a large extent, and surface fluxes are expected to generate the majority of coral $\delta^{18}O$ variance (Linsley et al., 1994).

3. Processes Affecting Seawater $\delta^{18}O$ and Salinity

We begin by examining the dominant dynamical influences on both salinity and $\delta^{18}O_{sw}$ in isoROMS. Figure 5 depicts the spatial patterns and temporal loadings associated with the first three principal components (PCs)

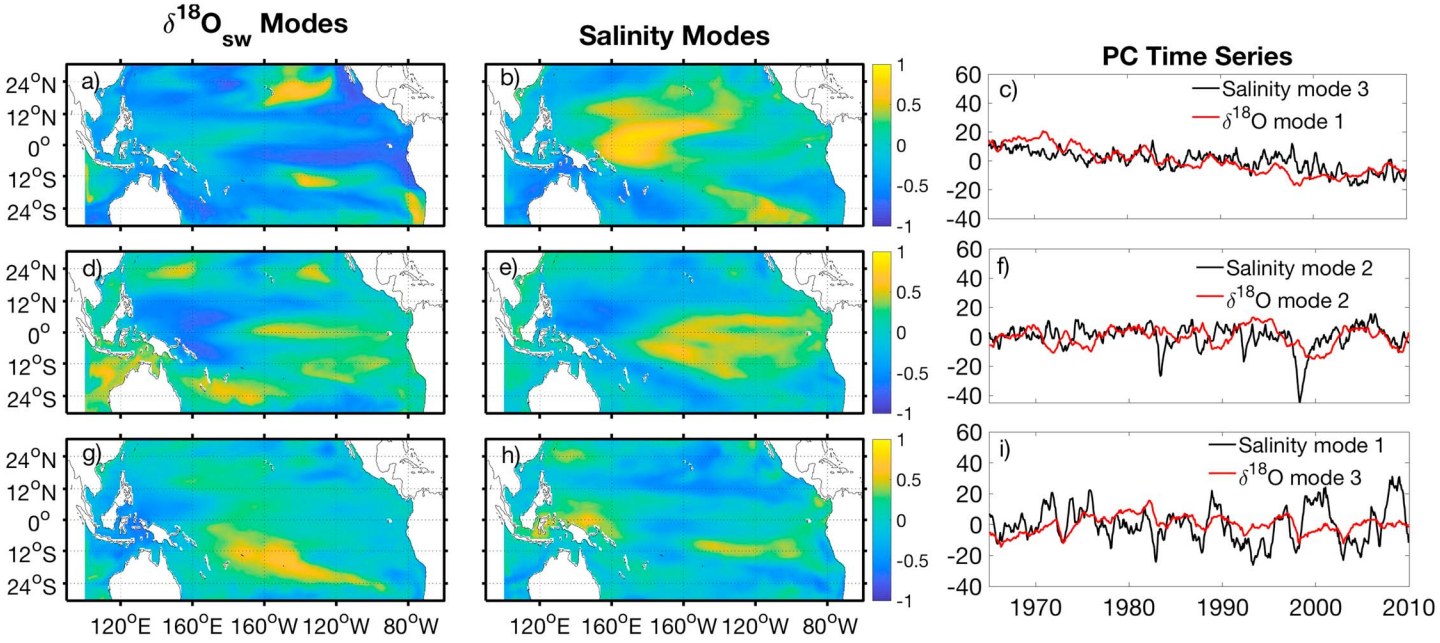

Figure 5. First three modes of variability in surface salinity anomaly and seawater $\delta^{18}O$ in isoROMS over 1965–2009. (a, b, d, e, g, h) Spatial patterns associated with modes. (c, f, i) Principal component (PC) time series associated with modes. Note that the signs of the PC time series have been reversed for some modes to illustrate covariability in salinity and $\delta^{18}O$ PCs (e.g., $\delta^{18}O$ mode 3).

of anomalies in both fields, calculated using monthly mean output from isoROMS. The first two salinity modes (Figures 5b, 5e, and 5h) are similar to those previously documented by Singh et al. (2011): the first mode resembles the salinity signature of the *Central* Pacific El Niño, explaining 22.5% of total variance and containing a tripolar structure along the equator. In contrast, the second mode (11.0% variance) contains a dipolar structure centered near 160°E, associated with variations of the SPCZ and Walker circulation during the eastern Pacific variety of El Niño. The third mode is associated with the salinity trend (8.15% variance), and the spatial pattern is consistent with previous observationally derived estimates of late twentieth century salinity trends (Cravatte et al., 2009; Durack et al., 2012).

The dominant empirical orthogonal functions (EOFs) of $\delta^{18}O_{sw}$ anomaly are calculated using the same methodology as for salinity and the results shown in Figures 5a, 5d, and 5g. Relative to salinity, the $\delta^{18}O_{sw}$ modes are ordered differently in terms of variance explained: the dominant mode is the trend, explaining 24.8% of the total variance. The western Pacific warm pool exhibits strong freshening (salinity)/depleting ($\delta^{18}O_{sw}$) trends, as does the ITCZ region; in contrast, saltening/enrichment is occurring in the subtropical South Pacific near 20°S. The larger proportion of variance explained by the trend mode in $\delta^{18}O_{sw}$ relative to salinity may indicate a role for evaporative enrichment/shifts in precipitation $\delta^{18}O$ structure in generating the trend.

A cross comparison of $\delta^{18}O_{sw}$ and salinity modes shows differences suggestive of varying hydrological influences on the two fields. For instance, the EOF pattern of $\delta^{18}O_{sw}$ mode 2 shows stronger anomalies over the warm pool than does salinity mode 2. This may reflect a higher sensitivity of $\delta^{18}O_{sw}$ to precipitative fluxes, as changes in the $\delta^{18}O$ of precipitation can sometimes play an important role. The $\delta^{18}O_{sw}$ pattern in mode 2 also shows more coherent structure over the ITCZ region, while salinity mode 2 features a more elongated loading extending from the warm pool into the SPCZ region. In both the warm pool and SPCZ regions, this suggests that hydrological effects of extreme El Niño events (Cai et al., 2014; Widlansky et al., 2013) may be mitigated in their $\delta^{18}O_{sw}$ expressions, potentially due to shifts in evaporative fractionation, and therefore that such events may not necessarily be efficiently recorded as $\delta^{18}O$ anomalies in coral records.

Differences in salinity/$\delta^{18}O_{sw}$ expressions of ENSO dynamics appear to affect the distinct behaviors of salinity mode 1 and $\delta^{18}O_{sw}$ mode 3. The PC time series of these modes correspond less well than the other PC pairs in Figure 5, and the equatorial centers of action in the EOF spatial patterns are noticeably offset from one another. The salinity mode 1 EOF features strongest loading near 160°E, consistent with the salinity expression of eastern Pacific El Niño events (see also Figure 7). In contrast, $\delta^{18}O_{sw}$ mode 3 has the peak of equatorial

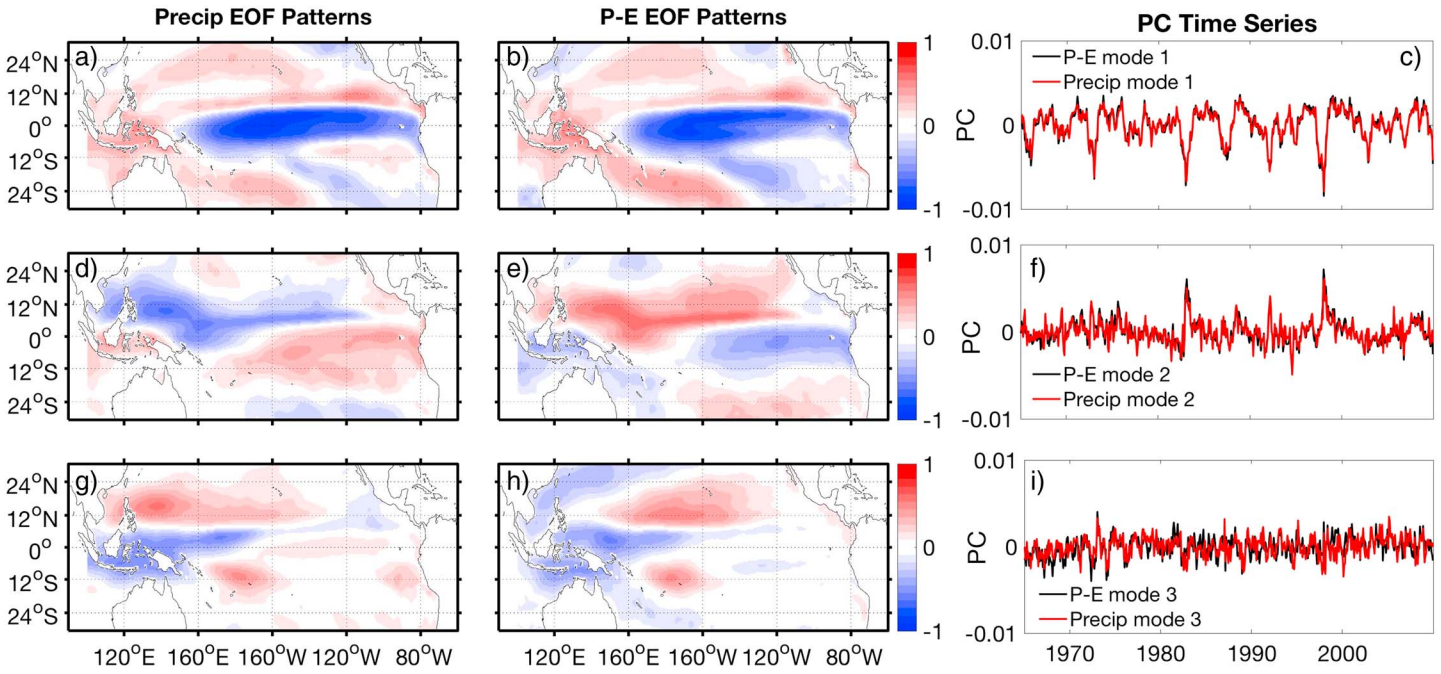

Figure 6. Same as Figure 5, for EOFs/PCs of precipitation and *P-E*. Again, some PC time series have been reversed for consistency (in this case, precipitation mode 2). EOF = empirical orthogonal function; PC = principal component.

variability closer to 130°E, near the Philippines. We hypothesize that this relates to the shift in atmospheric convection during El Niño events playing an enhanced role in generating far western Pacific $\delta^{18}O_{sw}$ relative to salinity anomalies.

It should be noted that for both salinity and $\delta^{18}O_{sw}$, the dominant modes of variability reflect a significant role for ocean dynamics; this highlights the need to move beyond the interpretation of $\delta^{18}O_{sw}$ variations as strictly surface driven (as previously noted by Stevenson et al., 2015, in the context of topographically driven upwelling around Christmas Island). To illustrate this point, Figure 6 shows the dominant modes of variability in precipitation and *P-E* anomalies, following the same conventions as Figure 5. ENSO teleconnection patterns are observable in mode 1, with spatial patterns distinct from salinity or $\delta^{18}O_{sw}$. Likewise, modes 2 and 3 reflect variations in ITCZ migration and convection over the warm pool but with unique spatial and temporal signatures. Also notable is the lack of a coherent trend in any of the three modes in Figure 6, suggesting that it may be possible to generate a secular $\delta^{18}O_{sw}$ trend without trends in surface freshwater fluxes.

Figure 7 shows the composite anomalies in temperature, salinity, and $\delta^{18}O_{sw}$ at the peak of both central Pacific and eastern Pacific El Niño events defined as in Yeh et al. (2009). These maps confirm that the expressions of El Niño in $\delta^{18}O_{sw}$ and salinity do differ in important ways: in particular, the anomaly in eastern equatorial Pacific salinity (Figure 7e) does not extend as far east in $\delta^{18}O_{sw}$ (Figure 7c) at the peak of eastern Pacific El Niño events. The largest similarities between salinity and $\delta^{18}O_{sw}$ appear in the central to western equatorial Pacific, a correspondence that will be discussed further in subsequent sections. The coral $\delta^{18}O$ patterns differ much more strongly between eastern and central Pacific El Niño years than do the $\delta^{18}O_{sw}$ fields, suggesting that temperature may be the dominant distinguishing factor in coral $\delta^{18}O$ signatures of ENSO diversity.

We next explore the dynamics of the features in Figure 7 by constructing the seawater $\delta^{18}O$ budget over the surface (0–10 m) layer. The procedure follows Stevenson et al. (2015), where the budget of seawater $\delta^{18}O$ is derived from the budgets of the individual isotopologue concentrations using the quotient rule. However, rather than using the budgets of the total isotopic ratio (*R*), the present analysis uses a Reynolds decomposition of the $H_2^{16}O$ and $H_2^{18}O$ budgets to derive the anomalous seawater $\delta^{18}O$ budget. This allows exploration of El Niño and La Niña influences relative to the seasonal cycle, as has been done extensively for temperature (Graham et al., 2014; Stevenson et al., 2017) and salinity (Hasson et al., 2013).

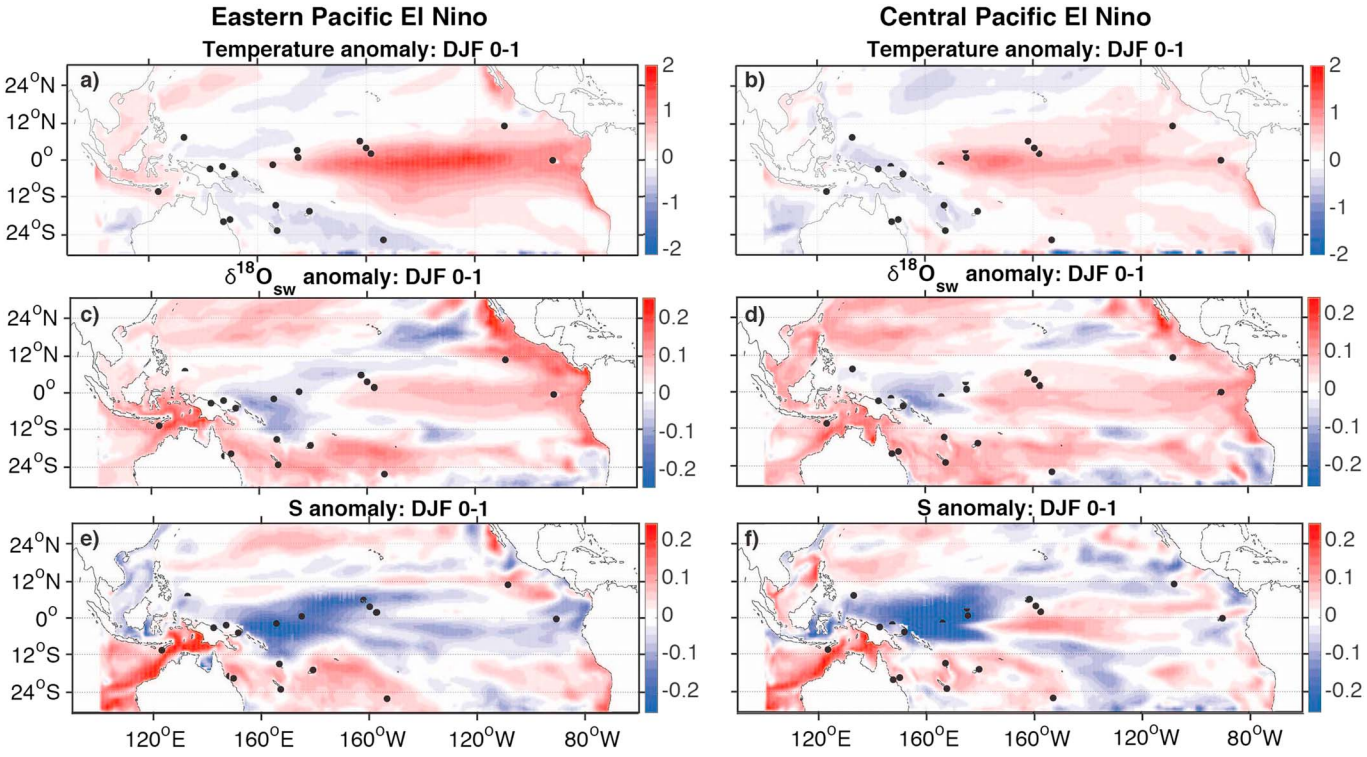

Figure 7. Composite (a, b) sea surface temperature, (c, d) seawater $\delta^{18}O$, and (e, f) salinity anomalies for eastern and central Pacific El Niño events, during DJF of the El Niño peak. Here "Year 0" refers to the year of event initiation, and "Year 1" to the following year, such that DJF of the El Niño peak occurs during the winter of Years 0–1. DJF = December-January-February.

We express the budgets of each isotopologue (here referred to generally as O or individually as either O_{16} or O_{18}) in the form

$$\frac{\partial O}{\partial t} = \Phi - \vec{v} \cdot \vec{\nabla} O + D \tag{2}$$

where Φ is the surface flux term and D is the term representing mixing/diffusion, calculated as the residual of all other terms. The Reynolds-decomposed form of the isotopologue budget is

$$\frac{\partial O'}{\partial t} = \Phi' - \bar{v} \cdot \vec{\nabla} O' - v' \cdot \vec{\nabla} \bar{O} - v' \cdot \vec{\nabla} O' + \overline{v' \cdot \vec{\nabla} O'} + D \tag{3}$$

The budget of the anomalous isotopologue ratio is

$$\frac{\partial R'}{\partial t} = \frac{\partial}{\partial t}\left[\frac{O_{18}}{O_{16}} - \left(\frac{\overline{O_{18}}}{O_{16}}\right)\right] = \frac{1}{O_{16}}\left[\frac{\partial O'_{18}}{\partial t} - R\frac{\partial O'_{16}}{\partial t}\right] \tag{4}$$

where the multiplicative factors contain the total time-varying values of O_{16} and R.

The individual terms in the R' budget can then be computed by substituting the relevant components of the isotopologue budgets into (3). When this is performed, Figure 8 shows the resulting contributions of each during the development phase of La Niña events and of Eastern Pacific El Niño events. The time rates of change are large in each case, particularly in the west/central equatorial and southwest Pacific, consistent with the expected patterns of seawater $\delta^{18}O$ during El Niño and La Niña events. The surface fluxes are extremely strong throughout the equatorial Pacific. However, in many locations these fluxes are mixed into the subsurface relatively rapidly; as such, we plot the surface contribution term here as the sum of flux and mixing/diffusion, to represent the net influence of surface processes on seawater $\delta^{18}O$.

A key insight from Figure 8 is the importance of advection. For example, although there is significant seawater $\delta^{18}O$ depletion during El Niño in the western/central equatorial Pacific (Figure 8a) and the reverse

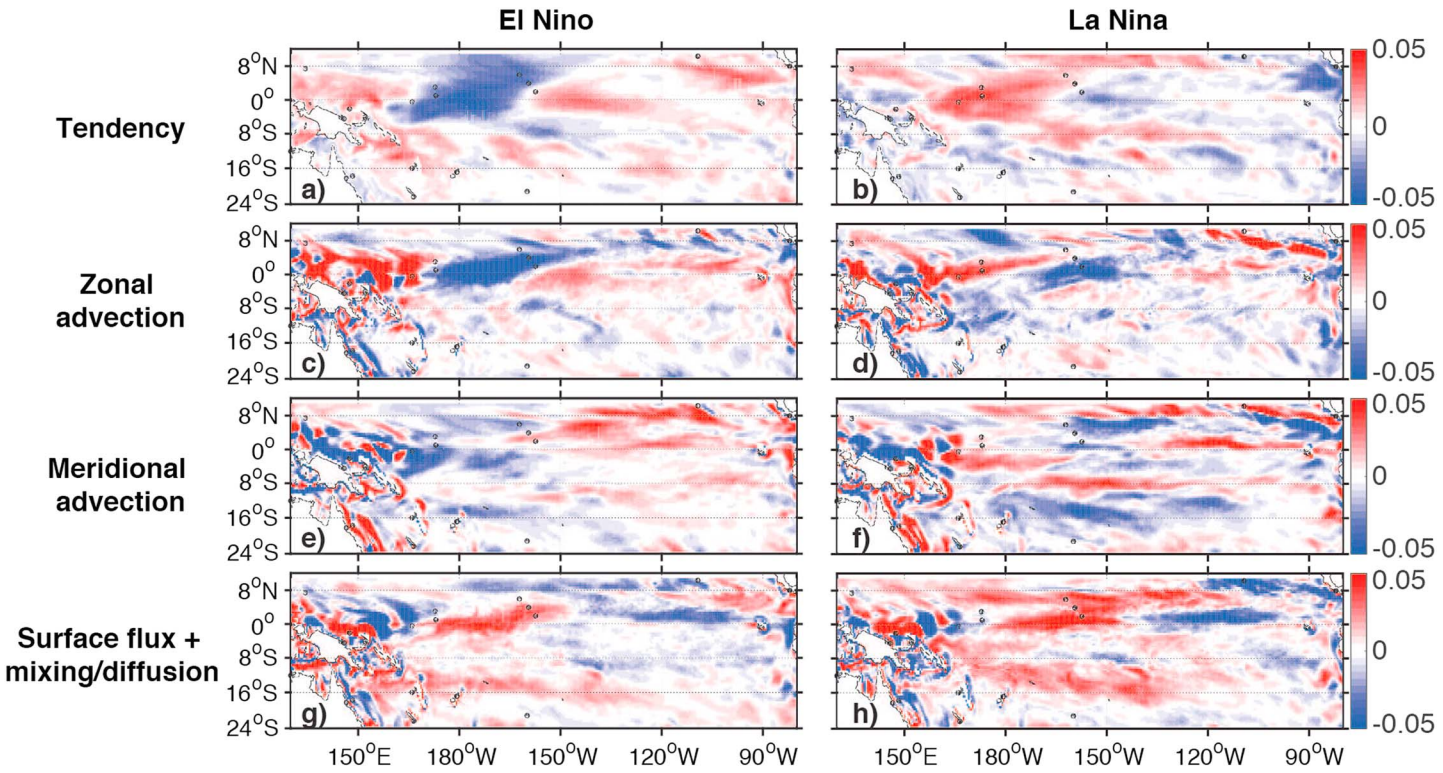

Figure 8. Terms in the $\delta^{18}O$ budget during JJA of eastern Pacific El Niño and La Niña development during 1965–2009. Units are per mil/month. JJA = June-July-August.

during La Niña (Figure 8b), the net surface influences tend to oppose these tendencies (Figures 8g and 8h). The dominant drivers of seawater $\delta^{18}O$ reduction in this region is zonal advection, with some contribution from meridional advection. This is consistent with previous budget analyses (Stevenson et al., 2015), as well as observational work at Butaritari showing significant correlations between $\delta^{18}O$ and surface currents (Carilli et al., 2014). Zonal advection is strong in this region due to the large seawater $\delta^{18}O$ gradient at the edge of the warm pool; the meridional gradients also appear to play a role. In both cases, contributions from both anomalous advection of mean gradients and mean advection of anomalies gradients are important, although are not depicted separately here in the interests of brevity.

4. The Seawater $\delta^{18}O$:Salinity Relationship

4.1. Spatial Structure

We next investigate how the distinct behaviors of salinity and $\delta^{18}O_{sw}$ affect relationships between the two variables, which is of key importance for forward model development. Figure 9 maps the regression slope derived from each individual ROMS surface grid point and shows a great deal of spatial structure, both zonally and meridionally. As suggested by LeGrande and Schmidt (2006; hereafter LG06), the salinity:seawater $\delta^{18}O$ slopes are higher in the South Pacific than in the equatorial region. At lower latitudes, precipitation $\delta^{18}O$ is relatively enriched, and so its impact on $\delta^{18}O_{sw}$ is minimal, while at higher latitudes the $\delta^{18}O$ of precipitation can be quite depleted and thus can produce a stronger change in $\delta^{18}O_{sw}$, which is more in line with changes in salinity. The zonal equatorial structure is also consistent with observational results (Conroy et al., 2017), with higher slopes in the western equatorial Pacific than the eastern: slopes in the west are in the range of 0.4‰/psu to 0.5‰/psu, while in the east slopes are nearer 0.1‰/psu. The cause for the enhanced western equatorial Pacific slope is likely the higher mean precipitation over the warm pool, which should tend to enhance covariance between salinity and seawater $\delta^{18}O$. In contrast, in the eastern equatorial Pacific, evaporative fractionation is more important, as is vertical mixing, which can have differential impacts on salinity and seawater $\delta^{18}O$. However, the salinity:seawater $\delta^{18}O$ slope varies substantially on spatial scales much smaller than the tropical Pacific or South Pacific taken as a whole. We note that the patterns in Figure 9 may vary somewhat due to processes operating on different temporal scales; temporal dependencies are discussed further in section 4.3.

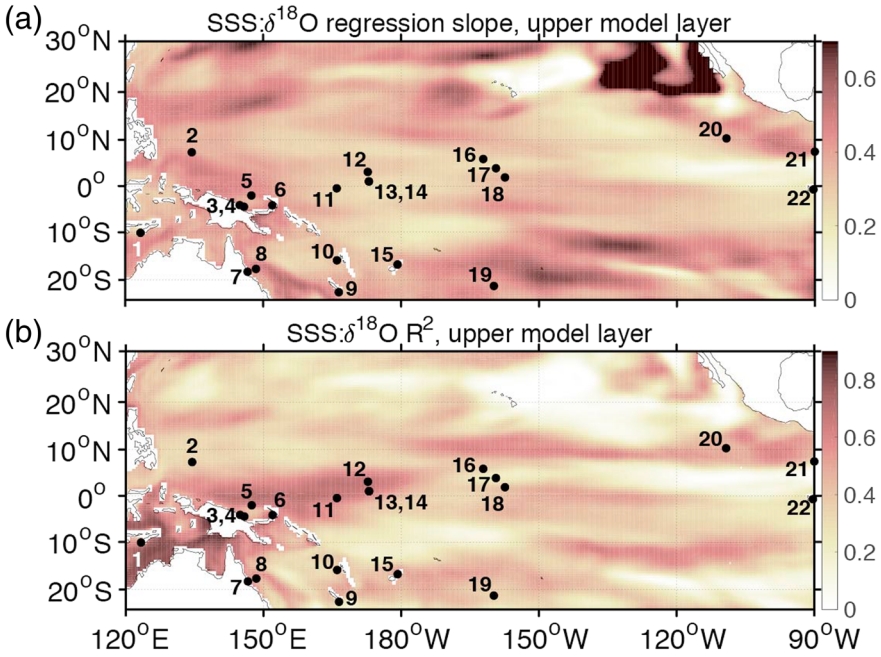

Figure 9. (a) Regression slope and (b) R^2 value for the SSS:seawater $\delta^{18}O$ relationship during 1965–2009. Numbers indicate proxy sites used in other analyses. SSS = sea surface salinity; 1 = Timor; 2 = Palau; 3 = Laing; 4 = Madang; 5 = Manus; 6 = Rabaul; 7 = Flinders; 8 = GBR; 9 = Amedee; 10 = Vanuatu; 11 = Nauru; 12 = Butaritari; 13 = Maiana; 14 = Tarawa; 15 = Fiji; 16 = Palmyra; 17 = Fanning; 18 = Christmas; 19 = Rarotonga; 20 = Clipperton; 21 = Secas; 22 = Galapagos.

4.2. Site-Specific Relationships

We next examine the structure of the salinity:seawater $\delta^{18}O$ relationship at individual sites. In Figures 10–12, monthly averaged salinity and seawater $\delta^{18}O$ in the upper model grid point closest to the coordinates of each study site are plotted for 1965–2009, and the best fit regression line derived from model output is shown alongside the regression from LG06. Here the LG06 slope is either the "tropical Pacific" (0.27‰/psu) or the "South Pacific" (0.45‰/psu) value, as indicated in the relevant panels. The best fit regression slopes for each individual site are listed in Table 2—it is immediately obvious that the slopes are similar overall to LG06 but that there is significant variation from site to site.

In Figures 10–12, El Niño, La Niña, and ENSO-neutral periods are plotted using distinct colors and plot symbols, which shows a diversity of responses in salinity:seawater $\delta^{18}O$ space across sites. Here El Niño and La Niña events are defined based on the NOAA classification, which uses the Oceanic NINO Index: El Niño winters are those encompassing January 1970, 1973, 1977, 1980, 1983, 1987, 1988, 1992, 1998, 2003, 2004, and 2007; likewise, La Niña winters are 1971, 1974, 1976, 1989, 1999, 2000, and 2008. For plotting purposes, El Niño and La Niña periods are defined as July–June centered on January of the years above, while all other times are considered ENSO-neutral.

The clearest ENSO signal in Figures 10–12 is seen in the west central Pacific sites, which show a relatively clean separation in phase space between El Niño and La Niña. Here El Niño is associated with low salinity and $\delta^{18}O$ values, with the converse during La Niña. This does not occur in the majority of sites in other categories, despite the overall positive correlations between seawater $\delta^{18}O$ and salinity. In fact, in many locations there does not appear to be a clear difference in salinity as a function of ENSO phase at all. This is likely due to the use of the full calendar year centered on El Niño-La Niña peaks, which may blur the ENSO signal in regions less strongly teleconnected than the west central Pacific sites.

The west central sites (Figure 11) show a slight tendency toward nonlinearity in their salinity:$\delta^{18}O_{sw}$ relation. This is evidenced by the fact that low-salinity values are accompanied by $\delta^{18}O$ values more negative than predicted by the linear fit, lending these plots a curved appearance. This effect is present but smaller at some warm pool sites (e.g., Laing, Madang, and Timor). At the west central sites, Figure 8 shows that the dominant contributor to $\delta^{18}O_{sw}$ depletion during El Niño development is zonal advection. This is therefore the most

Table 2
Regression Slopes β, Uncertainties on Regression Slopes Using a 36-Month Randomly Selected Window, and R^2 Values for Overall Salinity:Seawater $\delta^{18}O$ Relationships for the 1965–2009 Interval in isoROMS

Site	Class	β	β_{CI}	R^2
Flinders	Maritime Continent	0.49	+0.23/+0.63	0.50
GBR	Maritime Continent	0.43	+0.24/+0.53	0.52
Timor	Maritime Continent			
Butaritari	West Central Pacific	0.30	+0.11/+0.55	0.66
Maiana	West Central Pacific	0.26	−0.02/+0.40	0.64
Nauru	West Central Pacific	0.27	+0.10/+0.48	0.66
Tarawa	West Central Pacific	0.26	−0.03/+0.41	0.64
Clipperton	ITCZ	0.35	+0.21/+0.43	0.32
Secas	ITCZ	0.28	+0.20/+0.50	0.40
Laing	Warm pool	0.43	+0.14/+0.52	0.51
Madang	Warm pool	0.43	+0.12/+0.57	0.48
Manus	Warm pool	0.41	+0.22/+0.52	0.64
Palau	Warm pool	0.39	+0.17/+0.59	0.31
Rabaul	Warm pool	0.52	+0.22/+0.73	0.62
Christmas	Central Pacific	0.35	+0.18/+0.68	0.38
Fanning	Central Pacific	0.23	−0.12/+0.47	0.19
Palmyra	Central Pacific	0.29	+0.04/+0.53	0.38
Fiji	Southwest Pacific	0.38	+0.12/+0.47	0.38
New Caledonia	Southwest Pacific	0.34	0.00/+0.57	0.23
Rarotonga	Southwest Pacific	0.39	+0.13/+0.53	0.30
Vanuatu	Southwest Pacific	0.29	+0.06/+0.48	0.31
Galapagos	Eastern Pacific	0.19	+0.14/+0.30	0.20

Note. isoROMS = isotope-enabled Regional Ocean Modeling System; ITCZ = Intertropical Convergence Zone.

likely explanation for the nonlinear behavior of $\delta^{18}O_{sw}$ in Figure 11. We hypothesize that the strong precipitative anomalies near the warm pool edge modify the $\delta^{18}O_{sw}$ gradient more efficiently than the salinity gradient, creating enhanced $\delta^{18}O_{sw}$ anomalies relative to salinity. In contrast, Laing, Madang, and Timor lie in a domain strongly impacted by meridional advection (Figure 8). This is driven by the relaxation/strengthening of the trade winds during the ENSO cycle, enhancing/reducing the transport of low-$\delta^{18}O_{sw}$ waters away from the equator. The $\delta^{18}O_{sw}$ gradient is weaker meridionally than zonally, explaining the smaller magnitude of the nonlinearity at these sites relative to the west central grouping. Nonetheless, the coherent nature of this nonlinear behavior suggests the possibility for a nonlinear prediction based on salinity to provide an improved $\delta^{18}O_{sw}$ forward model.

At the southwest Pacific sites, the salinity:$\delta^{18}O_{sw}$ nonlinearity is not visually obvious. However, these sites show significant scatter overall, with a much larger range of seawater $\delta^{18}O$ values appearing for a given salinity. Based on Figure 8, the dominant influence on these sites during ENSO variations is surface flux changes, with some contribution from meridional advection. This could lead to scatter in the salinity:$\delta^{18}O_{sw}$ relation through variations in precipitation $\delta^{18}O$, the efficacy of subsurface mixing, or water mass exchanges across $\delta^{18}O_{sw}$ gradients (Linsley et al., 2006).

A high degree of scatter in the salinity:$\delta^{18}O_{sw}$ relationship is also observed in Figure 12 for the eastern and central Pacific, as well as the ITCZ, sites. In the ITCZ case, it is likely that variations in precipitative fluxes due to seasonal and ENSO variations are responsible for much of this; the importance of meridional advection in Figure 8 also suggests a role for water mass exchanges in affecting the salinity:seawater $\delta^{18}O$ relationship (a hypothesis also put forward for the Panama Bight region by Benway & Mix, 2004). For the eastern and central Pacific sites, the causes are likely both surface driven and dynamical. Strong ITCZ variations exist at Palmyra, for example, but meridional advection is also important here (Figure 8; Cobb et al., 2003). Subsurface mixing/diffusion are expected to be stronger at Christmas and Fanning due to their closer

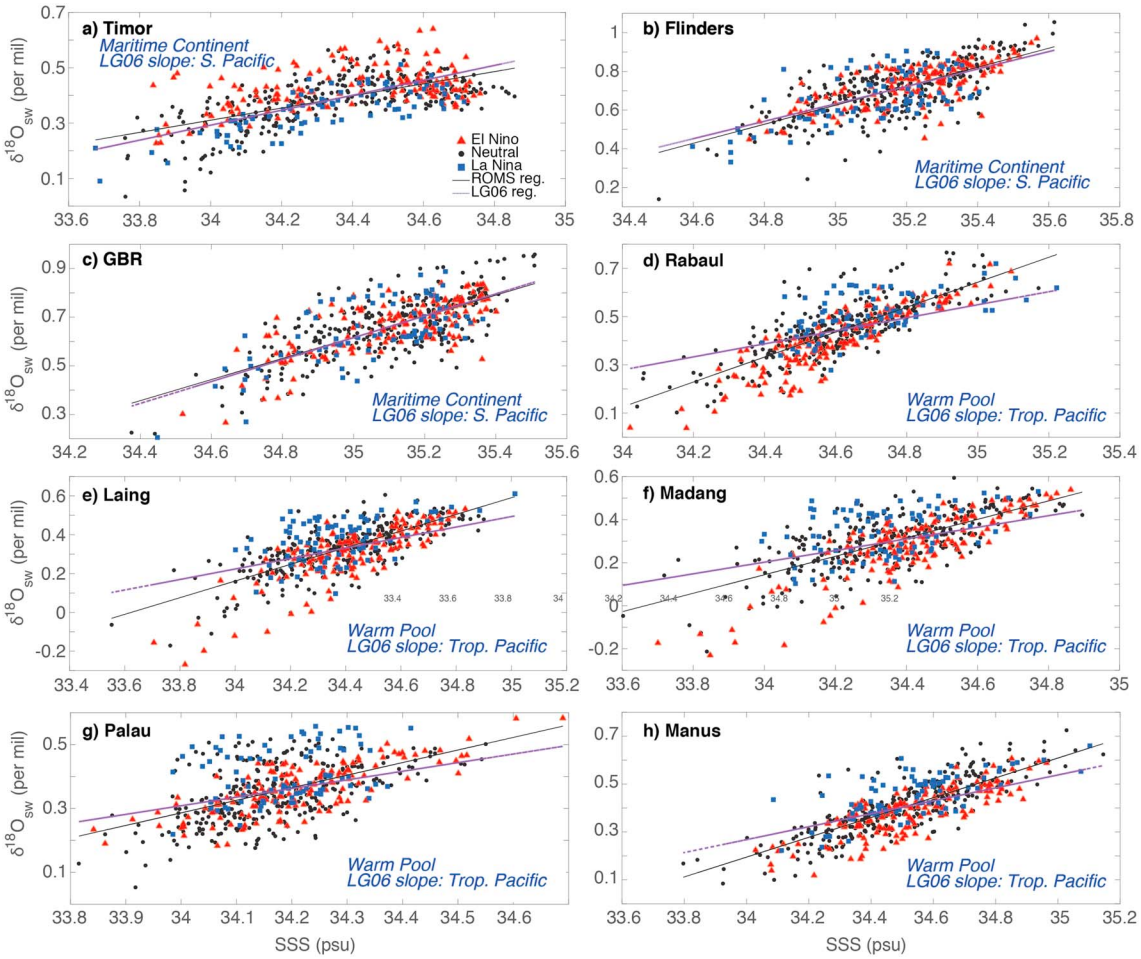

Figure 10. SSS:δ^{18}O relationships for monthly averaged Regional Ocean Modeling System (ROMS) output over the 1965-2009 period for Maritime Continent and warm pool sites. Red lines indicate the best fit linear regression slope from ROMS, while dashed black lines indicate the corresponding slope for either the "tropical" or "southern" Pacific from LeGrande and Schmidt (2006). SSS = sea surface salinity. (a) Timor; (b) Flinders; (c) Great Barrier Reef (GBR); (d) Rabaul; (e) Laing; (f) Madang; (g) Palau; and (h) Manus.

proximity to the equator (Nurhati et al., 2011), while at the Galapagos these processes may also be amplified by Equatorial Undercurrent variability (Karnauskas et al., 2010).

4.3. Temporal Stability

The final aspect of the seawater δ^{18}O:salinity relationship that must be considered is temporal variability. Particularly in locations where the ENSO signal is strong, the choice of study period may impact this slope by aliasing different levels of ENSO activity into the analyses. This is investigated qualitatively in Figure 13, which shows salinity:seawater δ^{18}O regression maps for three subintervals of the 1965–2009 period. Little change is observed in locations where the slope is already low (e.g., the eastern equatorial Pacific). However, strong modulation occurs in the central/western equatorial Pacific, near the Line Islands and the west central Pacific sites from Table 1. This highlights the importance of sustained monitoring efforts to adequately constrain long-term salinity and seawater δ^{18}O variations in the presence of possible "regime shifts" in the salinity:$\delta^{18}O_{sw}$ relationship.

As an estimate of the uncertainties arising solely from temporal variability, a Monte Carlo analysis has been performed for each of the study sites in Table 1. Here a random starting time is chosen within the 1965–2006 period and the salinity:seawater δ^{18}O regression slope computed for the 3-year period following that point. The choice of a 3-year interval is arbitrary but here chosen to represent typical lengths of salinity and δ^{18}O monitoring campaigns conducted to date (e.g., Conroy et al., 2017). Table 2 shows the 90% confidence intervals derived from 1,000 bootstrap samples using this approach. The slopes vary substantially at all sites, with a typical range of 0.2‰/psu to 0.6‰/psu—at most locations, the range of values encompasses both the

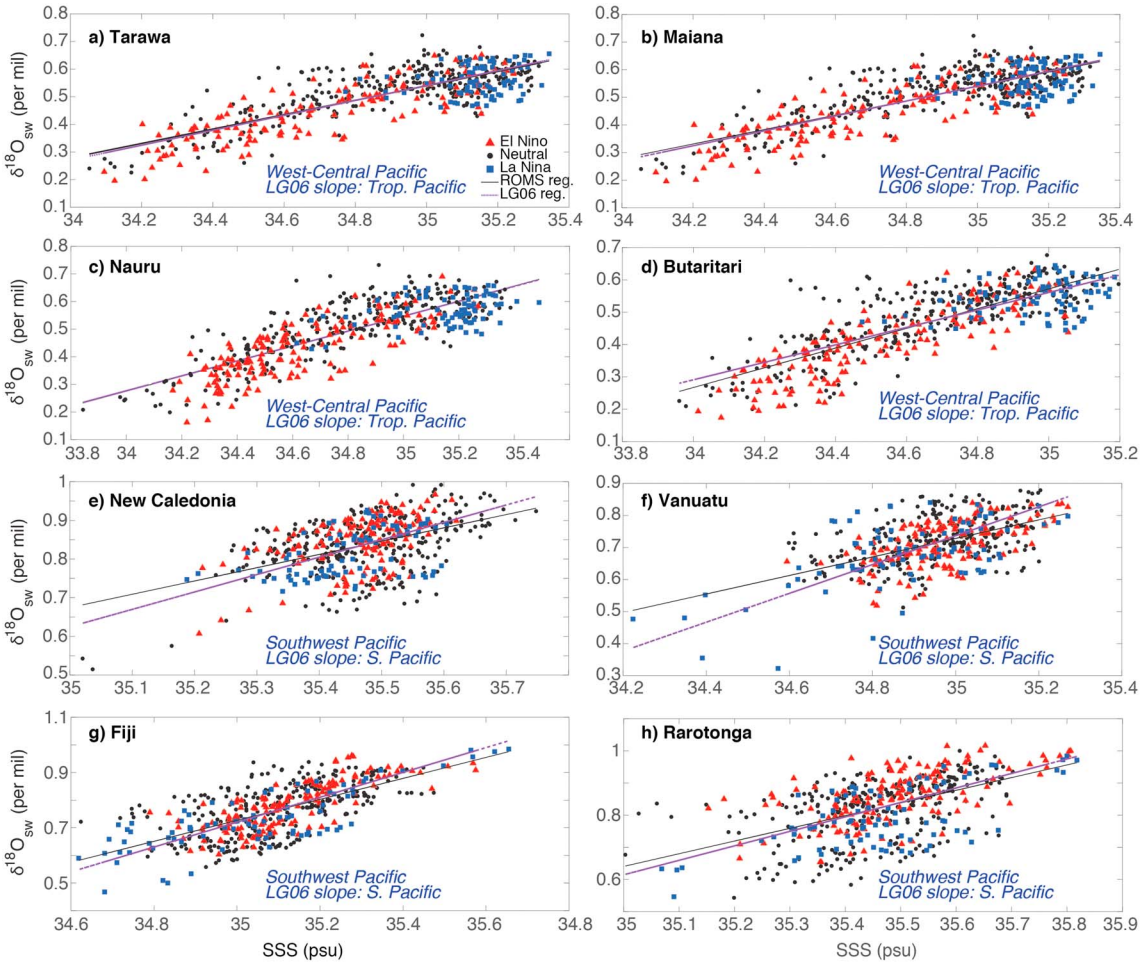

Figure 11. Same as Figure 10, for "west central" and "southwest Pacific" sites. (a) Tarawa; (b) Maiana; (c) Nauru; (d) Butaritari; (e) New Caledonia; (f) Vanuatu; (g) Fiji; and (h) Rarotonga.

tropical Pacific and South Pacific regional slopes computed by LG06. This is striking, as it indicates that at least on interannual time scales, the temporal variability in the salinity:seawater $\delta^{18}O$ relationship is actually larger than the spatial variability.

5. Discussion and Conclusions

The changing role of seawater $\delta^{18}O$ in generating variations in coral $\delta^{18}O$ on interannual time scales is a key uncertainty in coral-based ENSO reconstructions (Cobb et al., 2013). Without an accurate method for predicting both coral and seawater $\delta^{18}O$ as a function of ENSO dynamics, it is impossible to determine how well climate models represent the time history of ENSO; and in turn, without the ability to evaluate current salinity-based methods for predicting seawater $\delta^{18}O$ (Brown et al., 2008; Thompson et al., 2011), it is impossible to guide future improvements to coral forward modeling (Stevenson et al., 2013, 2015). Toward that end, this study has provided the first detailed dynamical analysis of controls on twentieth century seawater $\delta^{18}O$ in a physically realistic and spatiotemporally complete framework. These results thus complement existing studies based on observational data with limited extent (Conroy et al., 2014, 2017) and those using coupled model output (Russon et al., 2013), which may cover extremely long time scales but are subject to larger biases.

The relationship between salinity and seawater $\delta^{18}O$ in isoROMS is structurally similar to results from observations (Conroy et al., 2014, 2017; LeGrande & Schmidt, 2006), with lower slopes in the eastern equatorial Pacific relative to the central and western equatorial Pacific and higher slopes in the off-equatorial regions relative to the equatorial. However, the spatial structure of the regression relationship is quite complex, with variations

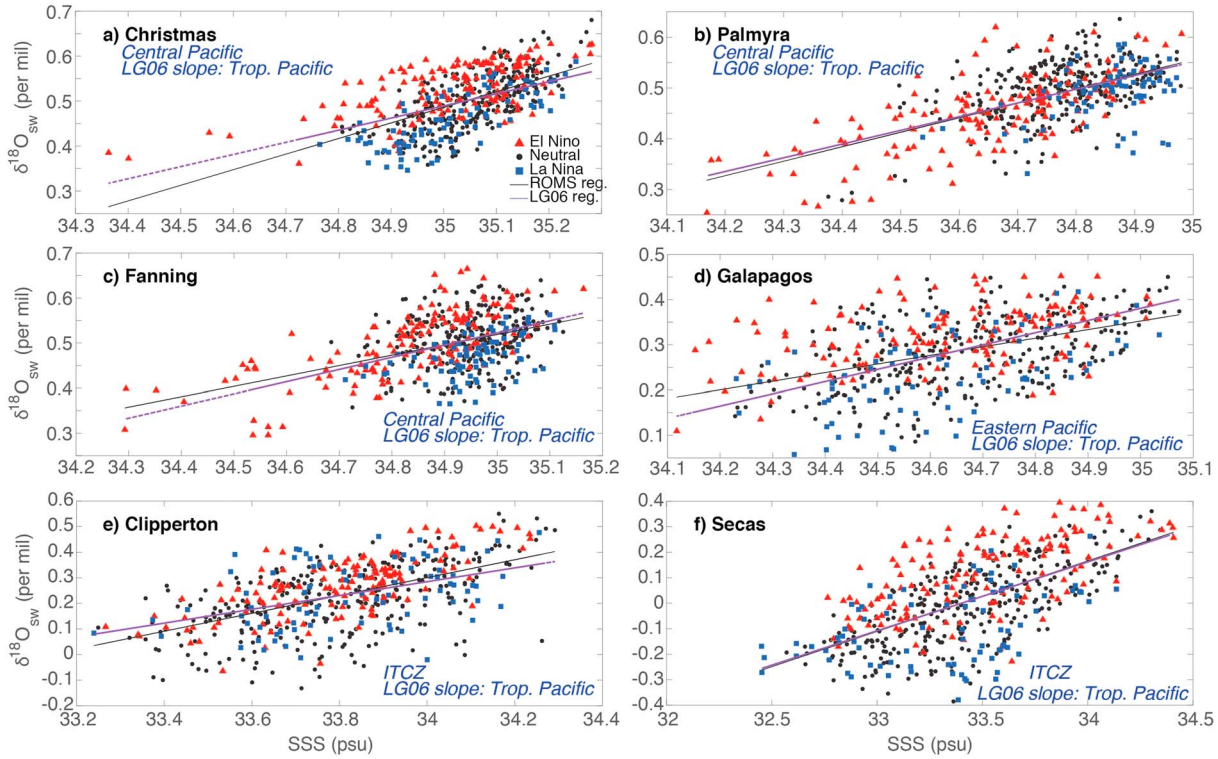

Figure 12. Same as Figure 10, for "central Pacific," "ITCZ," and "eastern Pacific" sites. ITCZ = Intertropical Convergence Zone. (a) Christmas; (b) Palmyra; (c) Fanning; (d) Galapagos; (e) Clipperton; and (h) Secas.

on spatial scales much smaller than suggested by LG06; slopes tend to be higher in regions directly impacted by the major tropical convergence zones, as well as in western equatorial Pacific locations with high climatological precipitation. The extremely low slopes observed in the eastern equatorial Pacific appear to result from strong vertical mixing and diffusive influences as well as shifts in water masses, which lead to differential salinity and seawater $\delta^{18}O$ responses and drive down covariance.

When examined at specific fixed study sites, the relationship between salinity and seawater $\delta^{18}O$ behaves quite differently in various circulation regimes. At equatorial sites near the edge of the warm pool ("west central Pacific" sites), salinity and seawater $\delta^{18}O$ covary quite strongly, and the local linear regression explains a substantial portion of the variance in $\delta^{18}O_{sw}$. This coherent relationship is driven primarily by zonal advective anomalies during the ENSO cycle, as the gradients in salinity and $\delta^{18}O_{sw}$ are strongly modified, as are anomalies in wind-driven currents. However, there is a noticeable nonlinearity in the relationship, with low-salinity periods associated with extremely negative seawater $\delta^{18}O$ values. In locations within the warm pool and under the ITCZ and SPCZ ("warm pool," "southwest Pacific," and "ITCZ" sites) no substantial nonlinearities are seen, but the scatter in the salinity:seawater $\delta^{18}O$ relationship is quite large. This appears to result from a combination of changes to precipitation $\delta^{18}O$, variations in subsurface mixing, and advective contributions. Finally, in the central/eastern equatorial Pacific ("eastern" and "central Pacific" sites), including the Line Islands chain which lies near the center of the NINO3.4 index region, there is both large scatter and substantial deviation from the overall relationship during ENSO extremes. The mechanisms for these influences differ from site to site within the eastern and central Pacific groupings, with enhanced contributions from equatorial upwelling/mixing at sites nearer the equator (Christmas, Galapagos) and contributions from precipitative fluxes and meridional advection more significant further from the equator (Palmyra). Such processes may help explain some of the observed spatial dependence of salinity:$\delta^{18}O_{sw}$ relationships (Conroy et al., 2017; LeGrande & Schmidt, 2006).

ENSO dynamics sometimes play a significant role in altering the salinity:$\delta^{18}O_{sw}$ relation, but this is not the case at all sites. At the west central Pacific sites (Figure 11), the salinity:seawater $\delta^{18}O$ relationship appears relatively coherent, indicating that salinity-based forward models should perform well regardless of ENSO phase and lending support to previous work in the region (Nurhati et al., 2009). However, in locations with large

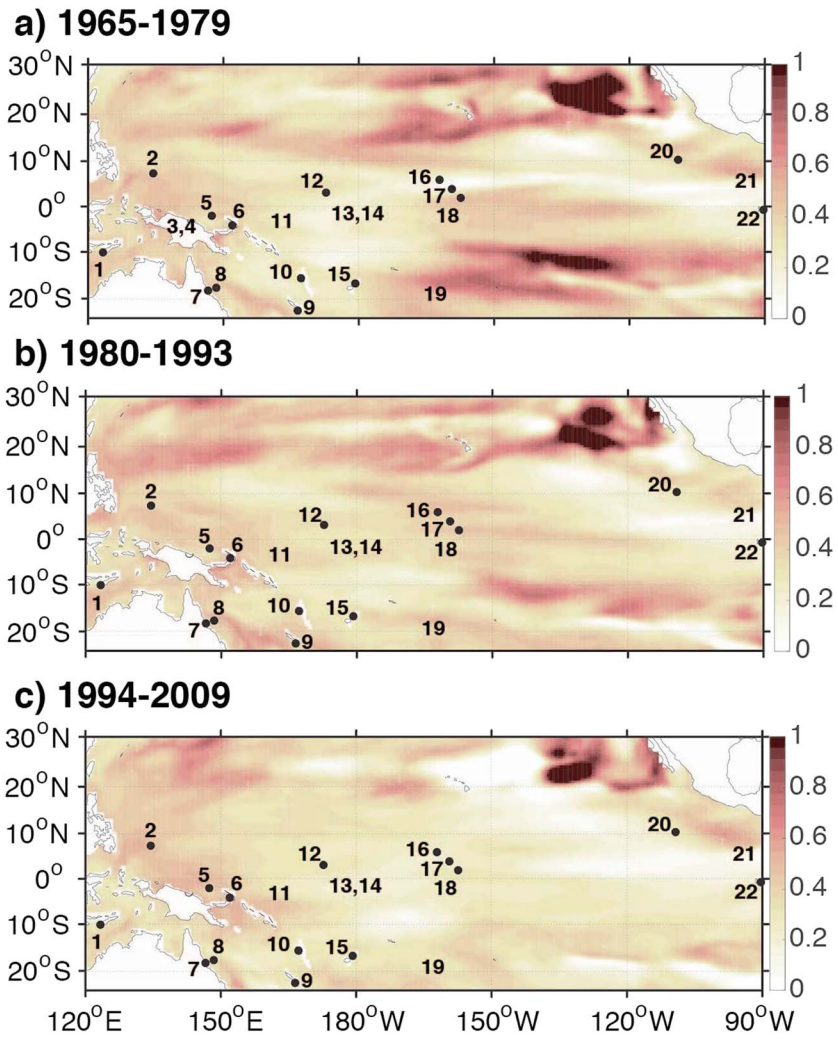

Figure 13. SSS:δ^{18}O relationships for isotope-enabled Regional Ocean Modeling System over three subintervals within the simulation period. Numbers indicate proxy sites used in other analyses. SSS = sea surface salinity; 1 = Timor; 2 = Palau; 3 = Laing; 4 = Madang; 5 = Manus; 6 = Rabaul; 7 = Flinders; 8 = GBR; 9 = Amedee; 10 = Vanuatu; 11 = Nauru; 12 = Butaritari; 13 = Maiana; 14 = Tarawa; 15 = Fiji; 16 = Palmyra; 17 = Fanning; 18 = Christmas; 19 = Rarotonga; 20 = Clipperton; 21 = Secas; 22 = Galapagos. (a) 1965–1979; (b) 1980–1993; and (c) 1994–2009.

scatter, a prediction of seawater δ^{18}O based on salinity (e.g., Thompson et al., 2011) may be strongly biased by ENSO variability within the study period—or simply unable to capture $\delta^{18}O_{sw}$ variance due to noise in the relationship. This suggests potential uncertainties in interpreting existing δ^{18}O records at these locations as representative of salinity (Dassie et al., 2018; Linsley et al., 2006). Finally, at some locations (in particular, Fanning, Madang, and Vanuatu) the slope of the salinity:seawater δ^{18}O relationship is also fundamentally different for ENSO-active periods, due to extreme salinity and δ^{18}O excursions related to El Niño or La Niña.

Although the major spatial features of the salinity:seawater δ^{18}O relationship are fairly stable through time, the values of the regression coefficients are not. Significant variations on decadal time scales are observed within ROMS, with the strongest changes seen in the central and western equatorial Pacific. Changes in coefficients are even larger on interannual time scales; a Monte Carlo analysis indicates that over an arbitrarily chosen 3-year period, the regression coefficient may change by up to 0.5‰/psu at most locations, likely owing to the action of the ENSO extremes occurring during that period.

These results have implications for the reconstructions both of ENSO and of paleosalinity (Conroy et al., 2017; Rohling & Bigg, 1998; Schmidt, 1999). The large temporal variability in the salinity:δ^{18}O slope implies that reconstructing past ENSO extremes may be associated with much larger uncertainties than previously

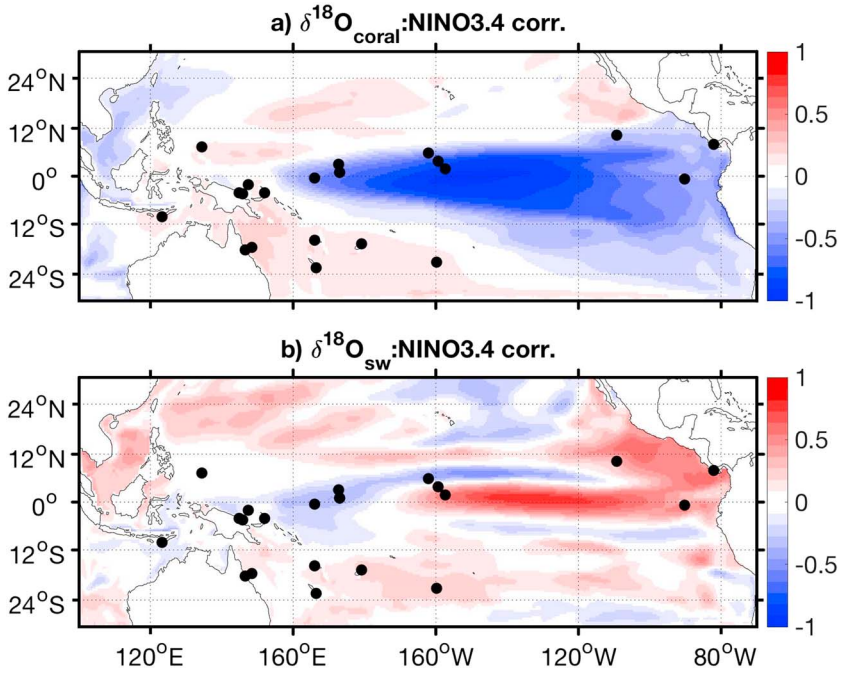

Figure 14. Correlation coefficient for (a) coral and (b) seawater $\delta^{18}O$ time series with the NINO3.4 index computed from isoROMS, over 1965–2009. Filled circles indicate study sites, as in Figure 13.

thought. Figure 14 shows the correlations between coral and seawater $\delta^{18}O$ and the NINO3.4 index in isoROMS; these coefficients do not always share the same sign, demonstrating that seawater $\delta^{18}O$ can have either a magnifying or damping influence on coral $\delta^{18}O$. If the seawater $\delta^{18}O$ component of $\delta^{18}O$ variability is not correctly represented in forward modeled $\delta^{18}O$ estimates from observations or climate models, the estimated ENSO extremes may therefore be overly large or small accordingly. Likewise, the reverse is true: using coral $\delta^{18}O$ records to extend observationally derived estimates of long-term salinity trends (Durack et al., 2012; Thompson et al., 2011) will be strongly influenced by these uncertainties as well. We note that these results are subject to caveats related to model performance; for further validation, both sustained monitoring efforts and additional model-based investigations are crucial for understanding the true extent of variability in the salinity:$\delta^{18}O_{sw}$ relationship and are highly recommended.

Acknowledgments
This work is supported by an NSF Ocean Sciences postdoctoral fellowship and a RAPID award to S. S., OCE-1323104 and OCE-1446930. Computing resources were provided by the Climate Simulation Laboratory at NCAR's Computational and Information Systems Laboratory (CISL) sponsored by the National Science Foundation and other agencies. Data from the isoROMS simulations presented here are available at https://doi.org/10.21424/R4PP8D.

References

Bailey, A., Toohey, D. W., & Noone, D. (2013). Characterizing moisture exchange between the Hawaiian convective boundary layer and free troposphere using stable isotopes in water. *Journal of Geophysical Research: Atmospheres*, *118*, 8208–8221. https://doi.org/10.1002/jgrd.50639

Bellenger, H., Guilyardi, E., Leloup, J., Lengaigne, M., & Vialard, J. (2014). ENSO representation in climate models: From CMIP3 to CMIP5. *Climate Dynamics*, *15*, 2013–9243. https://doi.org/10.1007/s00382-013-1783-z

Benway, H. M., & Mix, A. C. (2004). Oxygen isotopes, upper-ocean salinity, and precipitation sources in the eastern tropical Pacific. *Earth and Planetary Science Letters*, *224*(3-4), 493–507.

Brown, J., Tudhope, A. W., Collins, M., & McGregor, H. V. (2008). Mid-Holocene ENSO: Issues in quantitatve model-proxy data comparisons. *Paleoceanography*, *23*, PA3202. https://doi.org/10.1029/2007PA001512

Cahyarini, S. Y., Pfeiffer, M., Nurhati, I. S., Aldrian, E., Dullo, W.-C., & Hetzinger, S. (2014). Twentieth century sea surface temperature and salinity variations at Timor inferred from paired coral d^{18}O and Sr/Ca measurements. *Journal of Geophysical Research: Oceans*, *119*, 4593–4604. https://doi.org/10.1002/2013JC009594

Cahyarini, S. Y., Pfeiffer, M., Timm, O., Dullo, W.-C., & Schonberg, D. G. (2008). Reconstructing seawater $\delta^{18}O$ from paired coral $\delta^{18}O$ and Sr/Ca ratios: Methods, error analyses and problems, with examples from Tahiti (French Polynesia) and Timor (Indonesia). *Geochimica et Cosmochimica Acta*, *72*, 2841–2853.

Cai, W., Borlace, S., Lengaigne, M., van Rensch, P., Collins, M., Vecchi, G., et al. (2014). Increasing frequency of extreme El Niño events due to greenhouse warming. *Nature Climate Change*, *4*, 111–116. https://doi.org/10.1038/NCLIMATE2100

Carilli, J. E., Charles, C. D., Garren, M., McField, M., & Norris, R. D. (2013). Baseline shifts in coral skeletal oxygen isotopic composition: A signature of symbiont shuffling? *Coral Reefs*, *32*(2), 559–571.

Carilli, J. E., McGregor, H. V., Gaudry, J. J., Donner, S. D., Gagan, M. K., Stevenson, S., et al. (2014). Equatorial Pacific coral geochemical records show recent weakening of the Walker circulation. *Paleoceanography*, *29*, 1031–1045. https://doi.org/10.1002/2014PA002683

Cobb, K., Charles, C., Cheng, H., & Edwards, R. (2003). El Niño/Southern Oscillation and tropical Pacific climate during the last millennium. *Nature*, *424*, 271–276.

Cobb, K., Charles, C. D., Cheng, H., Edwards, R. L., Sayani, H. R., & Westphal, N. (2013). Highly variable El Niño-Southern Oscillation throughout the Holocene. *Science*, *339*, 67–70. https://doi.org/10.1126/science.1228246

Cole, J. E., Fairbanks, R. G., & Shen, G. T. (1993). Recent variability in the Southern Oscillation: Isotopic results from a Tarawa Atoll coral. *Science*, *260*, 1790–1793.

Collins, M., An, S.-I., Cai, W., Ganachaud, A., Guilyardi, E., Jin, F.-F., et al. (2010). The impact of global warming on the tropical Pacific Ocean and El Niño. *Nature Geoscience*, *3*, 391–397. https://doi.org/10.1038/NGEO868

Conroy, J. L., Cobb, K. M., Lynch-Stieglitz, J., & Polissar, P. J. (2014). Constraints on the salinity-oxygen isotope relationship in the central tropical Pacific Ocean. *Marine Chemistry*, *161*, 26–33. https://doi.org/10.1016/j.marchem.2014.02.001

Conroy, J. L., Noone, D., Cobb, K. M., Moerman, J. W., & Konecky, B. L. (2016). Paired stable isotopologues in precipitation and vapor: A case study within western tropical Pacific storms. *Journal of Geophysical Research: Atmospheres*, *121*, 3290–3303. https://doi.org/10.1002/2015JD023844

Conroy, J. L., Thompson, D. M., Cobb, K. M., Noone, D., Rea, A., & LeGrande, S. (2017). Spatiotemporal variability in the δ^{18}O-salinity relationship of seawater across the tropical Pacific Ocean. *Paleoceanography*, *32*(5), 484–497. https://doi.org/10.1002/2016PA003073

Cravatte, S., Delcroix, T., Zhang, D., McPhaden, M., & Leloup, J. (2009). Observed freshening and warming of the western Pacific warm pool. *Climate Dynamics*, *33*(4), 565–589.

Dassie, E. P., Hasson, A., Khodri, M., Lebas, M., & Linsley, B. K. (2018). Spatiotemporal Variability of the South Pacific Convergence Zone Fresh Pool Eastern Front from Coral-Derived Surface Salinity Data. *Journal of Climate*, *31*, 3265–3288.

Dassie, E. P., Linsley, B. K., Correge, T., Wu, H. C., Lemley, G. M., Howe, S., & Cabioch, G. (2014). A Fiji multi-coral δ^{18}O composite approach to obtaining a more accurate reconstruction of the last two-centuries of the ocean-climate variability in the South Pacific Convergence Zone region. *Paleoceanography*, *29*(12), 1196–1213. https://doi.org/10.1002/2013PA002591

Dee, S. G., Steiger, N. J., Emile-Geay, J., & Hakim, G. J. (2016). On the utility of proxy system models for estimating climate states over the common era. *Journal of Advances in Modeling Earth Systems*, *8*, 1164–1179. https://doi.org/10.1002/2016MS000677

Delcroix, T., Alory, G., Cravatte, S., Correge, T., & McPhaden, M. J. (2011). A gridded sea surface salinity data set for the tropical Pacific with sample applications (1950–2008). *Deep-Sea Research*, *58*, 38–48.

Di Lorenzo, E., & Mantua, N. (2016). Multi-year persistence of the 2014/15 North Pacific marine heatwave. *Nature Climate Change*, *6*, 1042–1047. https://doi.org/10.1038/nclimate3082

Durack, P. J., Wijffels, S. E., & Matear, R. J. (2012). Ocean salinities reveal strong global water cycle intensification during 1950 to 2000. *Science*, *336*(455), 455–458. https://doi.org/10.1126/science.1212222

Epstein, S., Buchsbaum, R., Lowenstam, H. A., & Urey, H. C. (1953). Revised carbonate/water isotopic temperature scale. *Geological Society of America Bulletin*, *64*(11), 1315–1326. https://doi.org/10.1130/0016-7606(1953)64[1315:RCITS]2.0.CO;2

Fairbanks, R., Evans, M., Rubenstone, J., Mortlock, R., Broad, K., Moore, M., & Charles, C. (1997). Evaluating climate indices and their geochemical proxies measured in corals. *Coral Reefs*, *16*, S93–S100.

Graham, F. S., Brown, J. N., Langlais, C., Marsland, S. J., Wittenberg, A. T., & Holbrook, N. J. (2014). Effectiveness of the Bjerknes stability index in representing ocean dynamics. *Climate Dynamics*, *43*, 2399–2414. https://doi.org/10.1007/s00382-014-2062-3

Guilderson, T. P., & Schrag, D. P. (1999). Reliability of coral isotope records from the western Pacific warm pool: A comparison using age-optimized records. *Paleoceanography*, *14*, 457–464.

Guilyardi, E., Wittenberg, A., Fedorov, A., Collins, M., Wang, C., Capotondi, A., et al. (2009). Understanding El Niño in ocean-atmosphere general circulation models: Progress and challenges. *Bulletin of the American Meteorological Society*, 325–340.

Hasson, A. E. A., Delcroix, T., & Dussin, R. (2013). An assessment of the mixed layer salinity budget in the tropical Pacific Ocean. Observations and modelling. *Ocean Dynamics*, 1990–2009. https://doi.org/10.1007/s10236-013-0596-2

Janeković, I., Powell, B. S., Matthews, D., McManus, M. A., & Sevadjian, J. (2013). 4D-Var data assimilation in a nested, coastal ocean model: A Hawaiian case study. *Journal of Geophysical Research: Oceans*, *118*, 5022–5035. https://doi.org/10.1002/jgrc.20389

Karnauskas, K., Murtugudde, R., & Busalacchi, A. (2010). Observing the Galápagos-EUC interaction: Insights and challenges. *Journal of Physical Oceanography*, *40*, 2768–2777.

Kilbourne, K., Quinn, T., Taylor, F., Delcroix, T., & Gouriou, Y. (2004). El Niño-Southern Oscillation-related salinity variations recorded in the skeletal geochemistry of a Porites coral from Espiritu Santo, Vanuatu. *Paleoceanography*, *19*, PA4002. https://doi.org/10.1029/2004PA001033.

Large, W. G., & Yeager, S. G. (2008). The global climatology of an interannually varying air-sea flux data set. *Climate Dynamics*, *33*, 341–364.

LeGrande, A. N., & Schmidt, G. A. (2006). Global gridded data set of the oxygen isotopic composition in seawater. *Geophysical Research Letters*, *33*, L12604. https://doi.org/doi:10.1029/2006GL026011.

Linsley, B. K., Dunbar, R. B., Wellington, G. M., & Mucciarone, D. A. (1994). A coral-based reconstruction of Intertropical Convergence Zone variability over Central America since 1707. *Journal of Geophysical Research*, *99*, 9977–9994.

Linsley, B., Kaplan, A., Gouriou, Y., Salinger, J., deMenocal, P., Wellington, G., & Howe, S. (2006). Tracking the extent of the South Pacific Convergence Zone since the early 1600s. *Geochemistry, Geophysics, Geosystems*, *7*, Q05003. https://doi.org/10.1029/2005GC001115

Linsley, B., Wellington, G., Schrag, D., Ren, L., & Salinger, M. (2004). Geochemical evidence from corals for changes in the amplitude and spatial pattern of South Pacific interdecadal climate variability over the last 300 years. *Climate Dynamics*, *22*, 1–11.

McGregor, H. V., Fischer, M. J., Gagan, M. K., Fink, D., & Woodroffe, C. D. (2011). Environmental control of the oxygen isotope composition of Porites coral microatolls. *Geochimica et Cosmochimica Acta*, *75*, 3930–3944.

Merlivat, L., & Jouzel, J. (1979). Global climatic interpretation of the deuterium-oxygen 18 relationship for precipitation. *Journal of Geophysical Research*, *84*(C8), 5029–5033.

Moerman, J. W., Cobb, K. M., Adkins, J., Sodemann, H., Clark, B., & Tuen, A. A. (2013). Diurnal to interannual rainfall δ^{18}O variations in northern Borneo driven by regional hydrology. *Earth and Planetary Science Letters*, *369-370*, 108–119.

Noone, D., & Simmonds, I. (2002). Associations between delta O-18 of water and climate parameters in a simulation of atmospheric circulation for 1979–95. *Journal of Climate*, *15*, 3150–3169.

Nurhati, I., Cobb, K., Charles, C., & Dunbar, R. (2009). Late 20th century warming and freshening in the central tropical Pacific. *Geophysical Research Letters*, *36*, L21606. https://doi.org/10.1029/2009GL040270

Nurhati, I. S., Cobb, K. M., & Di Lorenzo, E. (2011). Decadal-scale SST and salinity variations in the central tropical Pacific: Signatures of natural and anthropogenic climate change. *Journal of Climate*, *24*, 3294–3308.

Nusbaumer, J., Wong, T. E., Bardeen, C., & Noone, D. (2017). Evaluating hydrological processes in the Community Atmosphere Model Version 5 (CAM5) using stable isotope ratios of water. *Journal of Advances in Modeling Earth Systems*, *9*. https://doi.org/10.1002/2016MS000839

Osborne, M. C., Dunbar, R. B., Mucciarone, D. A., Druffel, E., & Sanchez-Cabeza, J.-A. (2014). A 215-yr coral d18O time series from Palau records dynamics of the west Pacific warm pool following the end of the Little Ice Age. *Coral Reefs*. Retrieved from https://doi.org/link.springer.com/article/10.1007/s00338-014-1146-1

Quinn, T. M., & Sampson, D. S. (2002). A multi-proxy approach to reconstructing sea-surface conditions using coral skeleton geochemistry. *Paleoceanography*, *17*(4), 1062. https://doi.org/10.1029/2000PA000528
Quinn, T. M., Taylor, F. W., & Crowley, T. J. (2006). Coral-based climate variability in the western Pacific warm pool since 1867. *Journal of Geophysical Research*, *111*, C11006. https://doi.org/10.1029/2005JC003243
Rohling, E. J., & Bigg, G. R. (1998). Paleosalinity and $\delta^{18}O$. *Journal of Geophysical Research*, *103*(C1), 1307–1318.
Ropelewski, C. F., & Halpert, M. S. (1987). Global and regional scale precipitation patterns associated with the El Niño/Southern Oscillation. *Monthly Weather Review*, *114*, 2352–2362.
Rozanski, K., Araguas-Araguas, L., & Gonfiantini, R. (1993). Isotopic patterns in modern global precipitation. In P. K. Swart et al. (Eds.), *Climate change in continental isotopic records, Geophysical Monograph Series* (Vol. 78, pp. 1–36). Washington, DC: American Geophysical Union.
Russon, T., Tudhope, A. W., Hegerl, G. C., Collins, M., & Tindall, J. (2013). Inter-annual tropical Pacific climate variability in an isotope-enabled CGCM: Implications for interpreting coral stable oxygen isotope records of ENSO. *Climate of the Past*, *9*, 1543–1557.
Schmidt, G. (1999). Error analysis of paleosalinity calculations. *Paleoceanography*, *14*(3), 422–429.
Schmidt, G., Hoffmann, G., Shindell, D., & Hu, Y. (2005). Modelling atmospheric stable water isotopes and the potential for constraining cloud processes and stratosphere-troposphere water exchange. *Journal of Geophysical Research*, *110*, D21314. https://doi.org/10.1029/2005JD005790
Schmidt, G., LeGrande, A., & Hoffmann, G. (2007). Water isotope expressions of intrinsic and forced variability in a coupled ocean-atmosphere model. *Journal of Geophysical Research*, *112*, D10103. https://doi.org/10.1029/2006JD007781
Shchepetkin, A., & McWilliams, J. (2005). The Regional Ocean Modeling System (ROMS): A split-explicit, free-surface, topography-following coordinates ocean model. *Ocean Modelling*, *9*(4), 347–404.
Singh, A., Delcroix, T., & Cravatte, S. (2011). Contrasting the flavors of El Niño/Southern Oscillation using sea surface salinity observations. *Journal of Geophysical Research*, *116*, C06016. https://doi.org/10.1029/2010JC006862
Souza, J., Powell, B., Castillo-Trujillo, A., & Flament, P. (2015). The vorticity balance of the ocean surface in Hawaii from a regional reanalysis. *Journal of Physical Oceanography*, *45*, 424–440. https://doi.org/10.1175/JPO-D-14-0074.1
Stevenson, S. (2012). Changes to ENSO strength and impacts in the CMIP5 models. *Geophysical Research Letters*, *39*, L17703. https://doi.org/10.1029/2012GL052759
Stevenson, S., Capotondi, A., Fasullo, J., & Otto-Bliesner, B. (2017). Forced Changes to Twentieth Century ENSO Diversity in a Last Millennium Context. *Climate Dynamics*. https://doi.org/10.1007/s00382-017-3573-5
Stevenson, S, Fox-Kemper, B., Jochum, M., Neale, R., Deser, C., & Meehl, G. (2012). Will there be a significant change to El Niño in the 21st century? *Journal of Climate*, *25*, 2129–2145. https://doi.org/10.1175/JCLI-D-11-00252.1.
Stevenson, S., Fox-Kemper, B., Jochum, M., Rajagopalan, B., & Yeager, S. (2010). Model ENSO validation using wavelet probability analysis. *Journal of Climate*, *23*, 5540–5547.
Stevenson, S., McGregor, H. V., Phipps, S., & Fox-Kemper, B. (2013). Quantifying errors in coral-based ENSO estimates: Towards improved forward modeling of δ^{18}O. *Paleoceanography*, *28*, 1–17. https://doi.org/10.1002/palo.20059
Stevenson, S., Powell, B., Merrifield, M., Cobb, K., Nusbaumer, J., & Noone, D. (2015). Characterizing seawater oxygen isotopic variability in a regional ocean modeling framework: Implications for coral proxy records. *Paleoceanography*, *30*, 1573–1593. https://doi.org/10.1002/2015PA002824
Thompson, D. M., Ault, T. R., Evans, M. N., Cole, J. E., & Emile-Geay, J. (2011). Comparison of observed and simulated tropical climate trends using a forward model of coral δ^{18}O. *Geophysical Research Letters*, *38*, L14706. https://doi.org/10.1029/2011GL048224
Tudhope, A. W., Chilcott C. P., McCulloch M. T., Cook E. R., Chappell J., Ellam R. M., et al. (2001). Variability in the El Niño/Southern Oscillation through a glacial-interglacial cycle. *Science*, *291*, 1511–1517.
Urban, F., Cole, J., & Overpeck, J. (2000). Influence of mean climate change on climate variability from a 155-year tropical Pacific coral record. *Nature*, *407*, 989–993.
Werner, M., Haese, B., Xu, X., Zhang, X., Butzin, M., & Lohmann, G. (2016). Glacial-interglacial changes in $H_2^{18}O$, HDO and deuterium excess—Results from the fully coupled ECHAM5/MPI-OM Earth system model. *Geoscientific Model Development*, *9*, 647–670.
Widlansky, M., Timmermann, A., Stein, K., McGregor, S., Schneider, N., England, M., et al. (2013). Shifted South Pacific rainfall bands in a warming climate. *Nature Climate Change*, *3*, 417–423.
Wittenberg, A. T. (2009). Are historical records sufficient to constrain ENSO simulations? *Geophysical Research Letters*, *36*, L12702. https://doi.org/10.1029/2009GL038710
Wu, H. C., Moreau, M., Linsley, B. K., Schrag, D. P., & Correge, T. (2014). Investigation of sea surface temperature changes from replicated coral Sr/Ca variations in the eastern equatorial Pacific (Clipperton Atoll). *Palaeogeography, Palaeoclimatology, Palaeoecology*, *412*, 208–222. https://doi.org/10.1016/j.palaeo.2014.07.039
Yeh, S.-W., Kug, J.-S., Dewitte, B., Kwon, M.-H., Kirtman, B. P., & Jin, F.-F. (2009). El Niño in a changing climate. *Nature*, *461*, 511–514. https://doi.org/10.1038/nature08316
Zhu, J., Zhengyu, L., Esther, B., Otto-Bliesner, B., Zhang, J., Noone, D., et al. (2017). Reduced ENSO variability at the LGM revealed by an isotope-enabled Earth system model. *Geophysical Research Letters*, *44*, 6984–6992. https://doi.org/10.1002/2017GL073406

Erratum

In the originally published version of this manuscript, author K.M. Cobb's name was published incorrectly. This error has since been corrected, and this can be considered the authoritative version of record.